

Review

Luminescent Metal Nanoclusters for Potential Chemosensor Applications

Muthaiah Shellaiah¹ and Kien Wen Sun^{1,2,*}

¹ Department of Applied Chemistry, National Chiao Tung University, Hsinchu 300, Taiwan; muthaiah1981@nctu.edu.tw

² Department of Electronics Engineering, National Chiao Tung University, Hsinchu 300, Taiwan

* Correspondence: kwsun@mail.nctu.edu.tw

Received: 21 November 2017; Accepted: 8 December 2017; Published: 19 December 2017

Abstract: Studies of metal nanocluster (M-NCs)-based sensors for specific analyte detection have achieved significant progress in recent decades. Ultra-small-size (<2 nm) M-NCs consist of several to a few hundred metal atoms and exhibit extraordinary physical and chemical properties. Similar to organic molecules, M-NCs display absorption and emission properties via electronic transitions between energy levels upon interaction with light. As such, researchers tend to apply M-NCs in diverse fields, such as in chemosensors, biological imaging, catalysis, and environmental and electronic devices. Chemo- and bio-sensory uses have been extensively explored with luminescent NCs of Au, Ag, Cu, and Pt as potential sensory materials. Luminescent bi-metallic NCs, such as Au-Ag, Au-Cu, Au-Pd, and Au-Pt have also been used as probes in chemosensory investigations. Both metallic and bi-metallic NCs have been utilized to detect various analytes, such as metal ions, anions, biomolecules, proteins, acidity or alkalinity of a solution (pH), and nucleic acids, at diverse detection ranges and limits. In this review, we have summarized the chemosensory applications of luminescent M-NCs and bi-metallic NCs.

Keywords: nanoclusters; fluorescent assay; nanosensors; bio-imaging; real analysis; colorimetric recognition; biomolecules detection; bi-metallic clusters

1. Introduction

Metal nanoclusters (M-NCs) have attracted the attention of the modern scientific community, because of their cost effective synthesis, biocompatibility, photostability, and wide applications [1–5]. M-NCs consist of few atoms (mostly between ten to hundred) of comparable sizes similar to the Fermi wavelength of electrons [6–8]. Hence, M-NCs can be considered as the missing link between single metal atoms and plasmonic metal nanoparticles [9]. In contrast to plasmonic nanoparticles, M-NCs have a size less than 2 nm [10,11] and do not exhibit any plasmonic characteristics. In addition, upon interaction with light, M-NCs display absorption and emission properties via electronic transitions between energy levels as in the case of organic molecules [12]. Therefore, in recent times, researchers have tended to apply M-NCs in various studies such as chemosensors, biological imaging, catalysis, as well as environmental and electronic devices. Chemo- and bio-sensory applications of luminescent M-NCs have attained most impressive progress [13–15].

Luminescent NCs of Au, Ag, Cu, and Pt have been successfully utilized as potential sensory materials [16–23]. Similar to organic fluorophores, carbon dots (CDs), and fluorescent quantum dots (QDs), luminescent M-NCs have been successfully applied in many sensor investigations because of their fluorescent nature, ultra-small size, and biocompatibility. Luminescent M-NCs have also been utilized in many in vivo/vitro biological imaging studies [24–27]. The stability of M-NCs has been improved using stabilizing agents.

The presence of templates on the surface of M-NCs can improve the stability and enhance sensing ability by providing a binding unit on the surface. For example, template-protected Au NCs have been previously reported as extended analytical tools for species detection [28]. These templates/stabilizers can also improve the luminescent property and biocompatibility of the clusters. Similar to Au NCs, other metal NCs (Ag, Cu, and Pt NCs) have displayed comparable fluorescent properties in the presence of various stabilizers [29–31]. Therefore, M-NCs are formed by reducing metal ions in the presence of appropriate reducing agents. Thiols, dendrimers, polymers, DNA oligonucleotides, peptides, and proteins have been commonly used to stabilize or improve the opto-electric properties of M-NCs [32].

Scholars have reported various applications of luminescent bi-metallic NCs. Bi-metallic NCs can be developed through different synthetic techniques, such as (1) galvanic replacement reaction, (2) anti-galvanic replacement reaction, (3) potential deposition, (4) thiol-etching of bi-metallic nanoparticles, and (5) re-organization of bi-metallic species [33]. To date, Au-Ag, Au-Cu, Au-Pd, and Au-Pt NCs have been utilized in various fields, such as catalysis, sensors, and bio-imaging. Overall, chemosensor applications of both M-NCs and bi-metallic NCs have attracted interest because of their cost-effective operation in biological and environmental samples.

Both metallic and bi-metallic NCs have been effectively applied to detect various analytes, such as metal ions, anions, biomolecules, proteins, pHs, and nucleic acids. Furthermore, metallic and bi-metallic NCs have also been reported as suitable candidates for bio-imaging. In this review, we summarize the chemosensory applications of luminescent M-NCs (M = Au, Ag, Cu, and Pt), as presented in Figure 1. In addition, we provide a brief note on the sensory applications of other M-NCs (such as Cd, Al, Pd, and Ir NCs) and bi-metallic NCs.

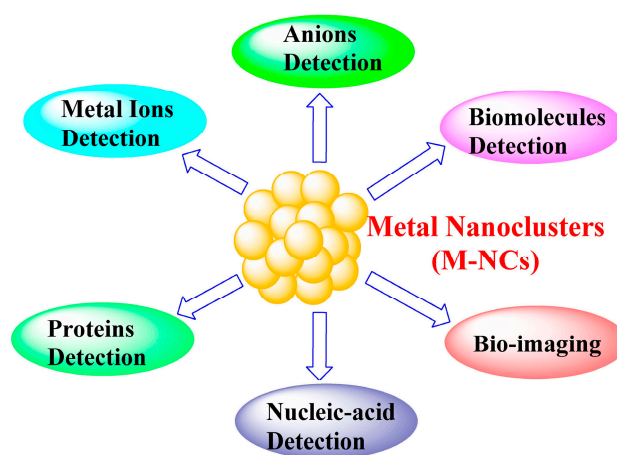


Figure 1. Schematic representation of chemosensor applications of metal nanoclusters (M-NCs).

2. Optimization Requirements

The sensory and bio-imaging applications of M-NCs are dependent on the following requirements, which must be optimized before designing such probes.

- A. **Ligands:** Suitable ligands must be selected to achieve enhanced fluorescence and tunable emissive colors, such as blue, green, red, orange, and yellow. Thiols, dendrimers, polymers, DNA-oligonucleotides, peptides, and proteins have been commonly used as ligands. Among them, ligands consisting of thiol groups have displayed outstanding results [34]. For example, Huang and Goswami's reports [35,36] on Au NCs described the use of thiolated ligands for capping. In both studies, diverse emissive colors were observed by optimizing the ligand or its concentrations. Several NC specimens are presented in this paper with various ligands, which have been already explored in many sensor studies. Thus, selection

of suitable ligands and optimization of their concentration play vital roles in the luminescent property of NCs.

- B. **Quantum Yield (Φ):** The quantum yield (Φ) of the probe should be effectively tuned by optimizing the reaction conditions, functionalizing the appropriate ligands at affordable concentration, and selecting solvents for assay methods to maximize the application of luminescent M-NCs in analyte detection. For example, Aldeek and Deng et al. presented Au NCs with polyethylene glycol with zwitterion and L-arginine functionalization and revealed diverse quantum yields of 14% and 65% [37,38]. Prof. Mattoussi and Chowdhury's research [39,40] on Ag NCs with diverse stabilizers demonstrated the enhancement of quantum yields. Lysozyme- and glutathione-stabilized Cu NCs have also been reported to have diverse quantum yields of 18% and 43%, respectively, for LED applications [41,42]. Fernández et al. presented lipoic-acid-capped Pt NCs with 47% quantum yields, which was due to the presence of a suitable stabilizer [43], thus confirming that an appropriate stabilizer affects the quantum yield or brightness of NCs.
- C. **Stability of NCs:** Stability is an important property that must be optimized prior to performing assay studies. Researchers verify the stability of their probes by using suitable stabilizers, solvents, temperatures, and pH levels [44]. Taylor et al. theoretically proposed thermodynamic stability [45] for design of M-NC-based probes for sensory and bio-imaging studies.
- D. **Toxicity:** The biological applications of M-NCs are attributed to toxicity optimization [46]. The probes must initially undergo MTT assay to authenticate their biocompatibility and intracellular permeability. Therefore, researchers have focused on developing less toxic M-NCs for drug delivery and imaging applications.

3. AuNCs in Sensor Studies

Among noble metal NCs, Au NCs seem more effective in biological and catalytic applications. Au NCs have been well utilized for detection of analytes, such as metal ions, anions, biomolecules, and DNA/RNA, and in in vitro/vivo cellular imaging of species. Here, we present a few examples of sensor applications. For metal ion sensors, Yang et al. developed lysine-stabilized Au NCs for detection of Cu^{2+} ions via fluorescence turn-off response (Figure 2). The results demonstrated that the method was highly sensitive, with a detection limit (LOD) of $0.8 \times 10^{-12} \text{ mol}\cdot\text{L}^{-1}$. In this study, the combination of Au NCs@Lys and Au NCs@BSA was utilized as a novel strategy for quantifying Cu^{2+} ions [47].

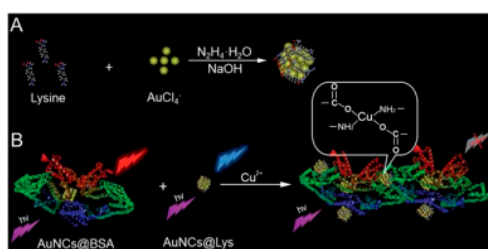


Figure 2. (A) Synthesis of Au NCs@Lys and (B) strategy for Cu^{2+} detection (Copyright Ref [47], Royal Society of Chemistry).

Using a similar approach, Deng et al. described biocompatible methionine-capped Au NCs (met-Au NCs) as a specific probe for detecting Cu^{2+} ions [48]. Cu^{2+} detection showed a linear range between 50 nM and 8 μM with a limit of 7.9 nM. The probe exhibited reversibility and improved selectivity among various metal ions and anions. These nanomolar LOD (limit of detection) with reversibility led to the development of such sensors in recent years. Metal-mediated Au NCs were further tuned to detect biomolecules via reversible fluorescent enhancement. For example, Wu et al. conveyed the “on–off–on” fluorescence recognition of Cu(II) and vitamin C [49]. Here, Au NCs

were templated with bovine serum albumin (BSA) to visualize the near-infrared fluorescence with a quantum yield of ~6.0%; these templated Au NCs have been effectively applied in HeLa cellular imaging of Cu^{2+} and vitamin C. Upon their functionalization with different precursors, Au NCs can specifically detect diverse metal ions.

Liu et al. presented the utility of α -chymotrypsin A (CTRA—which is an important enzyme in medical research) functionalized Au NCs for fluorometric and colorimetric sensing of Hg^{2+} ions [50]. In this study, Au NCs were synthesized by a “green method” and transferred to a cellulose membrane by realizing the advantage of blotting technology. The results suggested that the method can be applied as an alternative analytical tool for Hg^{2+} detection in research on life sciences and pollution. Senthamizhan et al. demonstrated the real-time visual recognition of Hg^{2+} ions in water at ppt level by using Au NC-decorated polycaprolactone (PCL) nanofibers [51]. Several research groups have developed cost-effective precursors to obtain stable Au NCs for sensory studies. For instance, Prof. Li’s group developed Au NCs stabilized by chicken egg white (CEW) for detection of Hg^{2+} ions [52]. These CEW-Au NCs selectively detected Hg^{2+} in the presence of Cu^{2+} ions by EDTA masking approach. Citrate-stabilized stannous ions (Sn(II)-citrate) have been used as reducing and capping agents to obtain Au NCs for simultaneous detection of Cu^{2+} and Hg^{2+} ions [53]. In this system, Chen et al. stated that Au NCs acted as dual spectroscopic probes that utilized both fluorescence (FL) quenched by Cu^{2+} and resonance light scattering (RLS) enhanced by Hg^{2+} ions.

Apart from Cu^{2+} and Hg^{2+} sensors, Au NCs with different stabilizers have also been used to detect other metal ions. Yang et al. reported red emitting $\text{Au}_7(\text{DHLLA})_2\text{Cl}_2$ clusters [54] with 3.6% quantum yield; the clusters were templated with dihydrolipoic acid (DHLLA) and acted as a potential fluorescent sensor for Fe^{2+} with an LOD of 3.8 μM (0.2 ppm). Moreover, this study proposed the dissociation-induced fluorescence quenching mechanism. Prof. Jin’s group used 11-mercapto-undecanoic acid (11-MUA) capped Au NCs ($\Phi = 2.4\%$) for exclusive detection of Cr(III) and Cr(VI) ions [55]. Upon the addition of Cr(III) to 11-MUA-Au NCs, the fluorescence intensity was quenched linearly between 25 and 10 mM with an LOD of 26 nM. The probe also detected Cr(VI) in the presence of ascorbic acid as a reductant in aqueous solution. Baral et al. established the detection of Fe^{3+} ions by Au NCs obtained from CTAB protected gold nanorods by using reduced glutathione [56]. These methods confirmed the reversibility of Fe(III) sensor with sulfide ions.

In contrast to previous works on Au NC-based metal ions sensors, Li et al. reported the fluorescent “turn-on” detection of Ag(I) ions [57] by employing BSA-protected small gold nanoclusters (Au_{16} NCs@BSA). As illustrated in Figure 3, upon the addition of Ag(I) ions to Au_{16} NCs@BSA, a blue shift and fluorescence enhancement were observed. This work proved that Au NCs may act as reductants for reducing Ag^+ into Ag^0 and to form hybrid Au@Ag NCs.

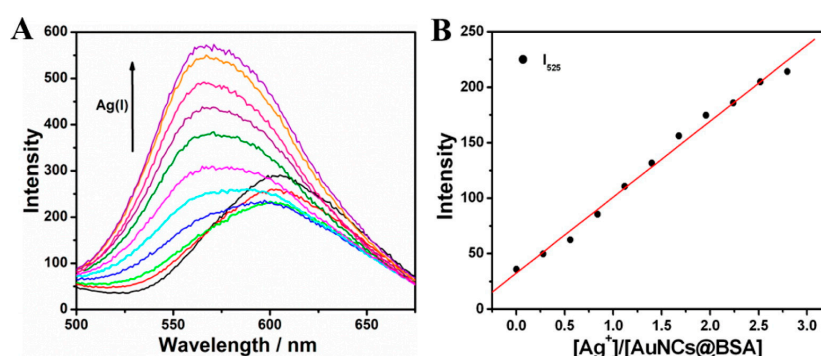


Figure 3. (A) Fluorescence spectra of Au_{16} NCs@BSA (1 mg/mL) in buffer solution (pH 7.5) measured 20 min after the addition of AgNO_3 ($\lambda_{\text{ex}} = 350$ nm), from bottom to top the concentration increasing from 0 to 40.0 μM . (B) Plot of photoluminescence (PL) intensity at 525 nm vs the molar ratio of Ag^+ to Au_{16} NCs@BSA; the concentrations of Ag^+ are the same as in (A) (Copyright Ref [57], American Chemical Society).

Au NCs with diverse precursors have also been used for selective recognition of anions. As presented in Figure 4, Liu et al. developed BSA-Au NCs for detection of CN^- ions [58]. This work presented the fluorescence quenching of BSA-Au NCs induced by CN^- ions with an LOD of 200 nM, which is ~ 14 times lower than the maximum cyanide level (2.7×10^{-6} M) allowed in drinking water by the World Health Organization (WHO). Moreover, this sensor was relatively simple and did not require any complex synthesis or complex instruments.

Zhang et al. and Shojaeifard et al. developed and applied red emitting Au NCs with Φ values of 1.03 and 0.13% in CN^- ion detection [59,60]. In these reports, L-amino acid oxidase (LAAOx) and L-glutathione (GSH) were used as agents to protect Au NCs. GSH-Au NCs [60] were initially titrated with copper(II) phthalocyanine [Cu(PcTs)]; analysis of the results revealed their turn-off effect on each other, leading to the recovery of [Cu(PcTs)] fluorescence in the presence of CN^- ions and the decrease in the fluorescence intensity of gold nanoclusters (Au NCs). Thereafter, researchers successfully applied BSA-protected Au NCs as probes for identifying anions, such as hypochlorite (HOCl), sulfide ion (S^{2-}), nitrite ion (NO_2^-), and pyrophosphate ion ($\text{P}_2\text{O}_7^{4-}$, PPI), with affordable linear detection ranges and limits [61–64]. Pyrophosphate ion ($\text{P}_2\text{O}_7^{4-}$, PPI) detection [64] was a fluorescent “turn-on” sensor via the BSA-Au NCs- Cu^{2+} mediated complex system. Sun et al. reported a similar approach for detecting PPI by forming a Fe^{3+} complex [65] with GSH/MUA protected clusters (Au NCs@GSH/MUA; $\Phi = 3\%$).

Acetylcysteine-stabilized gold NCs (ACC@Au NCs) with an excellent quantum yield of 14% have been recognized as selective and sensitive fluorescent sensors for detecting hydrogen sulfide (H_2S) [66]. Zhang et al. reported on H_2S detection over other anions, amino acids, and thiols (Figure 5). The ACC@Au NCs revealed a linear response between 0.002 and 120 $\mu\text{mol}\cdot\text{L}^{-1}$ with an LOD of 1.8 $\text{nmol}\cdot\text{L}^{-1}$. These impressive findings have highlighted Au NC-based biosensors.

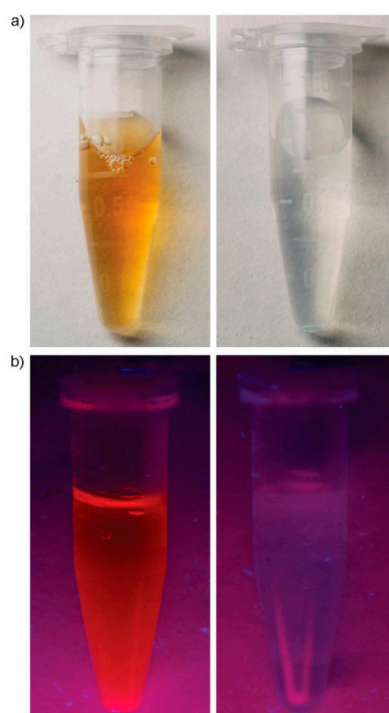


Figure 4. (a) Aqueous solution of Au NCs before (left) and after (right) addition of 5×10^{-3} M cyanide. (b) Fluorescence of the aqueous solution of Au NCs before and after addition of 5×10^{-3} M cyanide under UV light at 365 nm (Copyright Ref [58], WILEY publications).

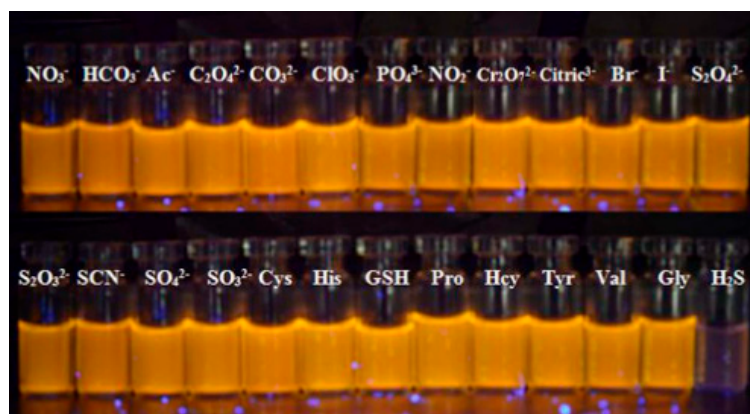


Figure 5. Photographs of acetylcysteine-stabilized gold NCs (ACC@Au NCs) with different analyte solutions viewed under UV light at 365 nm (Copyright Ref [66], ELSEVIER publications).

In addition to the detection of metal ions or anions, Au NCs have been exclusively applied for identification of biomolecules. BSA-templated Au NCs were effectively used as fluorescent probes for detecting cholesterol and dopamine [67,68]. In these studies, the utilized red emissive BSA-Au NCs became non-emissive during analyte recognition. Moreover, the LODs of cholesterol and dopamine were estimated to be 12 μM and 0.622 nM, respectively. Wen et al. utilized horseradish peroxidase (HRP)-templated Au NCs for detection of hydrogen peroxide [69]. The linear assay range was 100 nM to 100 μM with an LOD of 30 nM. This study can be extended to other functional proteins to produce dual functional NCs by mixing the functions of biomolecules and nanoclusters via a simple one-step synthesis. In addition to these sensor studies, Ni^{2+} ion-mediated BSA-Au NCs were employed as attractive probes for “turn-on” detection of histidine over other amino acids [70]. This work used human urine samples for real-time monitoring, and the recoveries ranged from 95% to 104%. Dai et al. presented a metal-mediated approach, in which Hg^{2+} -mediated BSA-Au NCs were used for determination of melamine [71]. The sensor LOD decreased to 0.15 mM (which is 130 times lower than the estimated value by the US Food and Drug Administration). This work also demonstrated the practicality of melamine detection in raw milk and milk powder.

Song and Chen et al. reported the use of peptide- and BSA-capped Au NCs for sensing protein kinase activity (which plays a significant role in adjusting cellular biological processes) and quercetin (a flavonoid present in Chinese Herbal Medicine), respectively [72,73]. During sensor titration, both cases revealed fluorescence quenching with LODs of $0.004 \text{ U}\cdot\text{mL}^{-1}$ (U is defined as the enzyme quantity that liberates 1 μg or μM of the product) and $1.8 \times 10^{-8} \text{ mol}\cdot\text{L}^{-1}$, correspondingly. Wu et al. presented the use of GSH-Au NCs for detecting heparin (which plays a crucial role in the regulation of various biological processes, such as cell growth and differentiation, inflammation, immune defense, lipid transport, and metabolism) [74]. This report demonstrated the detection of heparin in the presence of cetyl-trimethyl ammonium bromide (CTAB, fluorescence enhancing agent) with a limit of $0.075 \text{ mg}\cdot\text{mL}^{-1}$. This probe (GSH-Au NCs) was also applied to detect human serum samples.

Bioimaging studies of fluorescent Au NCs have also gained considerable interest in recent years. In view of their fluorescent quantum yield, biocompatibility, and photostability, template-protected Au NCs have been utilized as novel optical probes for in vitro and in vivo fluorescence imaging studies [75]. For example, purine-stabilized green fluorescent Au NCs with 1.2% quantum yield in methanol were used in cell nuclei imaging studies [76].

In a previous study, Au NCs were treated with HeLa, A498, Schwann, and L929 cell lines to confirm their nucleus targeting ability; the results showed green emission from their nuclei (Figure 6). Wang et al. demonstrated the “turn-on” bio-imaging ability of near-infrared (NIR) fluorescent Au NCs ($\Phi = 7.7\%$)/graphene oxide nanocomposites in cancer cells and small animals [77]. In a similar manner, *Caenorhabditis elegans* (free-living round worms in temperate soil environments that lack respiratory

and circulatory systems) and reactive oxygen species (ROS) were imaged with mulidendate thiolated tryptophan- and BSA-capped Au NCs [78,79]. In both studies, the NIR-fluorescence had quantum yields of 6% and 5.8% and was effectively used in the imaging readings. Biswas et al. employed Au NCs containing polymeric microcapsules to investigate the intracellular ratiometric fluorescence biosensing response to hydrogen peroxide [80].

As in the case of organic fluorescent probes, Au NC-based probes also acted as pH-sensitive probes in chemo- and bio-sensor investigations [81,82]. For example, Wu et al. reported a dual-emission fluorescent probe consisting of BSA-Au NCs and fluorescein-5-isothiocyanate (FITC) as temperature and pH sensors [83]. The probe displayed temperature sensing from 21 °C to 41 °C and pH from 6.0 to 8.0. Ali et al. indicated the use of BSA-Au NCs as pH-selective sensors within the pH range of 5 to 9 [84].

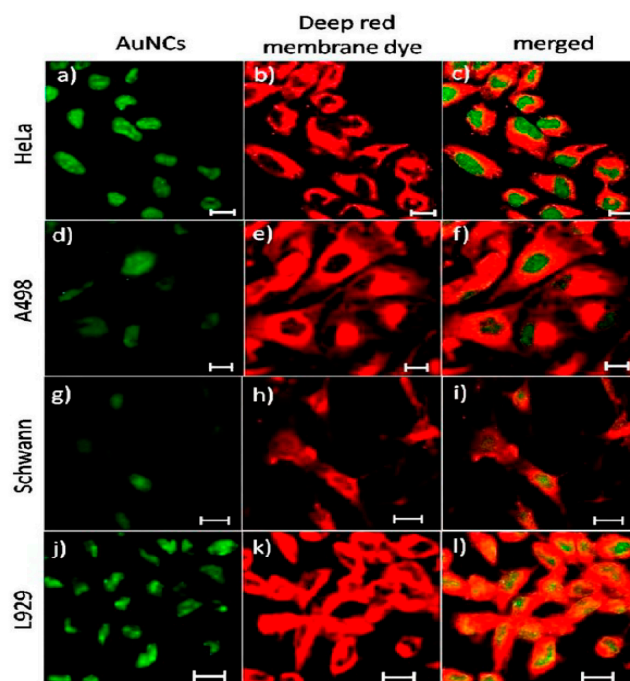


Figure 6. Confocal laser scanning microscope images of four different cell lines after treatment with green emitting AuNCs ($\lambda_{em} = 510$ nm); deep red plasma membrane dye exhibits red emission ($\lambda_{em} = 633$ nm), which is used as a reference for cell membrane staining. (a–c) Images of Au NCs, deep red plasma membrane dye, and their merged images of HeLa cells, respectively. (d–f) Images of A498 cells; (g–i) images of Schwann cells; (j–l) images of L929 cells (scale bar corresponds to 10 μ m) (Copyright Ref [76], American Chemical Society).

4. Ag NCs as Sensory Probes

As noble metal NCs, Ag NCs have attracted the attention of the scientific community because of their extraordinary sensory performance. Given their high fluorescent quantum yield, biocompatibility, and photo and chemo stability, Ag NCs have been applied in various sensory investigations. Luminescent Ag NC-based metal ions sensors are the most notable [85]. In the past decade, Shang et al. elucidated Ag NCs-based fluorescent detection of Cu(II) ions [86] in a linear range of 1.0×10^{-8} to 6.0×10^{-6} M; the obtained LOD was found to be as low as 8 nM. In this work, poly(methacrylic acid) (PMAA) was utilized as a template and stabilizer. Fluorescence quenching-based recognitions of Cu(II) ions have been achieved by hyper branched poly-ethyleneimine (hPEI)- and amido black 10B (AB)-stabilized Ag NCs ($\Phi = 1.5\%$ and 0.2) [87,88]; the LODs were estimated as 10 and 4 nM, respectively. Sun et al. presented GSH-passivated Ag NCs for specific fluorimetric and colorimetric recognition of Cu(II) ions [89]. This work presented both the fluorimetric and colorimetric responses of GSH-Ag NCs to Cu(II) ions (Figure 7) and demonstrated the reversibility in the presence of EDTA.

These GSH-Ag NCs showed subnanomolar LODs in both responses (0.050 nM in fluorimetric and 0.60 nM in colorimetric) with reasonable linear ranges.

Adhikari et al. reported on Hg(II) ion detection in water by dihydrolipoic acid (DHLA) stabilized Ag NCs ($\Phi = 2\%$ in water) [90]. This work established Hg(II) detection via the fluorescence quenching of NIR-Ag NCs. The linear range was from 10^{-8} to 10^{-5} M with an LOD of 10^{-10} M, which is lower than the maximum permissible limit in drinking water (2 ppb, 10 nM). DNA-templated Ag NCs were successfully applied in Hg(II) sensor studies by MacLean and Yin's research groups [91,92]. In both investigations, diverse DNA sequences were utilized, resulting in fluorescence quenching and enhanced responses during Hg(II) ion recognition. The LODs of the Hg(II) sensors by both probes were estimated as 4 nM and 0.08 nM, respectively. Lee et al. also presented DNA-based Ag clusters (Cyt₁₂-Ag NCs; $\Phi = 43.9\%$) for detection of Ag(I) ions [93]. In this study, Cyt₁₂-Ag NCs validated the recognition of Ag(I) ions through the shift of the fluorescence response from red to green with an LOD of 10 nM. Furthermore, the Ag(I) sensor selectivity was confirmed through the detection of Ag⁺ in Silmazin (dermatological burn ointment containing silver sulfadiazine).

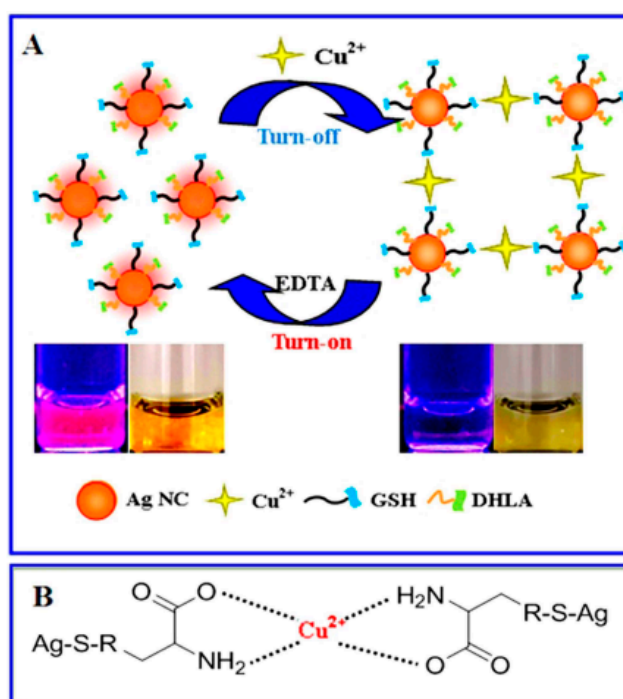


Figure 7. Schematic illustration of (A) the reversible fluorimetric and colorimetric detection mechanism and procedure of L-glutathione (GSH)-passivated Ag NCs toward the fluorimetric and colorimetric assays for Cu²⁺ ions (insert: the photographs of corresponding products), and (B) the chelating interaction between Cu²⁺ ions and GSH of GSH-passivated Ag NCs (Copyright Ref [89], Nature Publications).

Polyethyleneimine (PEI)- and GSH-capped Ag NCs have been extensively applied for detection of Cr(VI), Fe(III), and Pb(II) ions with affordable LODs [93–96]. However, GSH@Ag NCs for detection of Pb(II) ions were synthesized by a sonochemical method [96] rather than a wet chemical route. These probes exhibited fluorescence quenching during determination of metal ions. Liu et al. used DNA-stabilized Ag NCs for ratiometric recognition of mercury and copper ions [97]. The linear ranges of Hg²⁺ and Cu²⁺ were from 0.01 μ M to 0.5 μ M and from 0 μ M to 1.0 μ M with corresponding LODs of 1.03 nM and 2.77 nM, respectively. This work also discriminated the detections in the presence of an EDTA chelating reagent. To date, many studies have developed probes for detection of other analytes.

Ag NCs have also been exploited for anion discovery. Chen et al. developed blue-emitting GSH-stabilized Ag NCs ($\Phi = 1.9\%$) through a sonochemical method and successfully applied them in sulfide ion (S^{2-}) detection [98]. The recognition of S^{2-} ions also revealed fluorescent quenching with an LOD of 2 nM. Gao et al. performed S^{2-} ion detection by utilizing denatured lysozyme-capped clusters (dLys-Ag NCs) [99]. They tuned the molar ratios of $AgNO_3$ to lysozyme (1:1, 2:1, and 4:1 for synthesizing dLys-Ag NCs 1, 2, and 3, respectively) and then used them in sensor titrations. Furthermore, S^{2-} ion detection via “turn-off” and “turn-on” responses was realized by dLys-Ag NCs (1) and dLys-Ag NCs (3), respectively, with LODs of 0.2 and 0.6 $\mu\text{mol}\cdot\text{L}^{-1}$, respectively. Moreover, these probes were effective in real water samples. Huang et al. employed Ag NC-capped silica nanoparticles ($SiO_2@Ag$ NCs) for photoluminescent ratiometric quantification of S^{2-} and I^- ions, with LODs of 62 and 57 nM, respectively [100].

Hyperbranched polyethyleneimine-protected silver nanoclusters (hPEI-Ag NCs) were reported by Chen et al. for recognition of nitrite (NO_2^-) ion [101]. The involved NO_2^- sensor was validated by the fluorescent “turn-off” response of the cluster material. This study used the nitrite– H_2O_2 chemical reaction as a detection principle. The LOD of the sensor was estimated as 100 nM with a linear range of 0 to 7 μM . Wang et al. proposed a solvent induced fluorescent enhancement strategy for identification of I^- ions in urine samples [102].

In this work, upon addition of isopropyl alcohol (IPA), the fluorescence of GSH-Ag NCs was enhanced and then addressed in I^- detection via the “turn off” response with the limit of 0.5 nM (Figure 8). This probe was also applied in urine sample analysis with an LOD of 7.5 nM. The simultaneous detection of iodide (I^-) and bromide (Br^-) ions was realized by carboxymethyl dextran (CMD)-stabilized Ag NCs [103]. In this report, the probe was applied to detect I^- in the presence of Br^- in an ammonia medium, and the total amounts of Br^- and I^- ions were measured in a Britton–Robinson (BR) buffer solution. Liu et al. used lysozyme-stabilized Ag NCs (dLys-Ag NCs) as probes for the ratiometric detection of hydrogen peroxide and hydroxyl radical with live cell imaging [104]. The linear detection range for H_2O_2 was from 0.8 to 200 $\mu\text{mol}\cdot\text{L}^{-1}$ with an LOD of 0.2 $\mu\text{mol}\cdot\text{L}^{-1}$. This probe was also applied in H_2O_2 -generated oxidase-based biosensing. For instance, this probe involved the discovery of glucose and acetylcholine chloride with LODs of 0.6 and 0.8 $\mu\text{mol}\cdot\text{L}^{-1}$. Moreover, the hydroxyl radical fluctuation was verified by cellular imaging. Thus, the development of such probes was still focused on the effective utility in the findings of hydroxyl-induced oxidative damage in proteins.

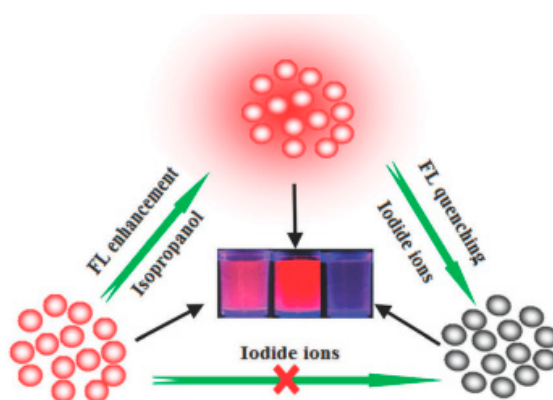


Figure 8. Schematic illustration of isopropyl alcohol (IPA)-triggered fluorescence enhancement of the Ag NCs and then fluorescence turning-off induced by iodide ions (Copyright Ref [102], Royal Society of Chemistry).

Templated Ag NCs have also been significantly applied in the detection of biologically important species. For example, Liu et al. used L-GSH stabilized Ag NCs with a quantum yield of 9.09% for the chiral recognition of amino acids [105]. They used the fast and green micro wave-assisted approach to

develop water-soluble fluorescent L-GSH-Ag NCs. In addition, DNA-templated AgNCs ($\Phi = 18.6\%$) were used as probes for identifying thiol compounds, such as GSH, cysteine (Cys), and homocysteine (Hcy) via fluorescent enhancement [106]. This report also revealed the order of enhancement as Hcy > GSH > Cys. Zhang et al. employing polyethyleneimine-capped silver nanoclusters (PEI-Ag NCs; $\Phi = 3.81\%$) in the assay of important biothiol compounds in the presence of various interferences [107]. This sensor probe was more specific for the identification of Cys, Hcy, and GSH via fluorescent “turn-off” (Figure 9). The obtained linear ranges for Cys, Hcy, and GSH were 0.1–10 mM, 0.1–10 mM, and 0.5–6 mM, respectively, with the LODs of 42, 47, and 380 nM. Moreover, during the addition of biothiol compounds to the probe, color changes from colorless to red-brown were observed, which can be visualized through naked eyes without any complex instruments.

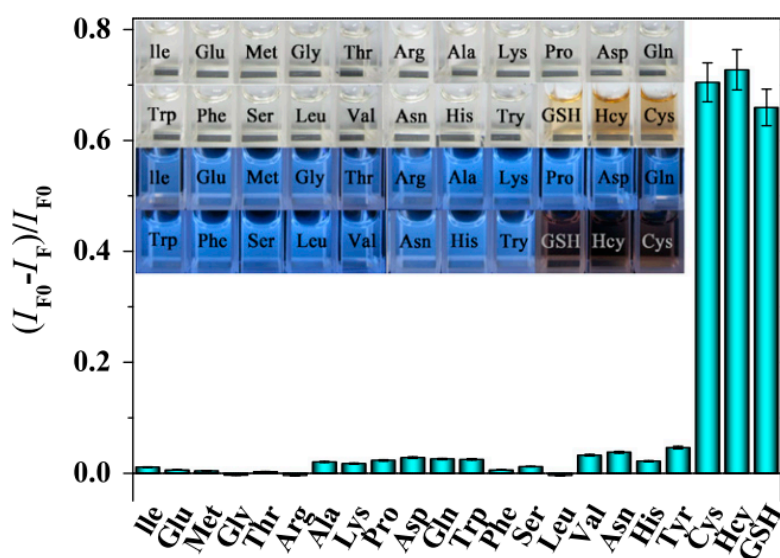


Figure 9. The responses of different amino acids to polyethyleneimine (PEI)-capped Ag NCs: Cys, Hcy and GSH (10 mM), other 19 amino acids (100 mM). The picture inserted shows the color and fluorescence change of Ag NCs to different amino acids (300 mM) (Copyright Ref [107], ELSEVIER publications).

In view of the requirement of specific analyte sensors, Yuan et al. exploited GSH-Ag NCs ($\Phi = 4.2\%$) for Cys detection [108]. Red-emitting GSH-Ag NCs were used for Cys detection via PL quenching over 19 other non-thiol containing amino acids with an LOD of 3 nM. Zhu et al. used the GSH-Ag NCs probe by controlling the molar ratio between Ag and glutathione for Cys detection through the tunable dual-emission fluorescent sensitivity [109]. For cluster-based biomolecule detection, Dong et al. reported on the discovery of urea and glucose by utilizing GSH-Ag NCs [110]. The GSH-Ag NCs displayed pH switchable agglomeration, leading to fluorescent quenching in the pH range of 3.57–8.05. This ability was beneficial for the sensing of urea and glucose through the “off-on” responses. The detections had linear ranges of 5–170 μM and 0.3–13 mM with LODs of 10 nM and 10 μM , respectively.

In this footpath, Jin et al. used chromotropic acid (CTA) and layered double hydroxide nanosheets-functionalized Ag NCs (CTA-Ag NCs/LDH; $\Phi = 12.08\%$) as an effective “off-on” sensor for melamine [111]. This probe can determine melamine in the concentration range of 0.03 mM to 0.1 mM with an LOD of 4 nM. Chen et al. realized fluorometric “turn-on” glucose detection by Ag NCs based on the Fenton reaction, which can trigger the clusters [112]. This approach is a new strategy for glucose detection. Mao et al. used polyethyleneimine-capped Ag NCs combined with Cu^{2+} ions, which act as a metal mediated precursor for the selective recognition of quinolones present in biologically important antibiotics [113]. This assay presented the “turn-on” sensor for the trace detection of quinolones with the use of a PEI-Ag NCs- Cu^{2+} system with good linear ranges and low LODs.

Similar to small-biomolecules detection, DNA-templated Ag NCs with a high fluorescent quantum yield of ~60% have also been applied in the recognition of specific proteins, such as thrombin [114]. Zhou et al. repeatedly used the DNA aptamer stabilized yellow emissive Apt-Ag NCs (Φ value of ~17%) for the selective detection of prion protein [115]. The probe confirmed the higher selectivity to prion (PrP^c) than that to other proteins, such as HSA, BSA, lysozyme, thrombin, and pepsin, at 10-fold higher concentrations than PrP^c. In the same way, DNA-Ag NCs have been successfully used in the selective determination of bleomycin (glycopeptide-derived antibiotics isolated from *Streptomyces verticillus*), which was then applied in cancer treatment [116]. However, the probe became more active in the presence of Fe²⁺ ions. Moreover, the linear detection range of bleomycin was estimated at 100–400 nM with an LOD of 54 nM. In a similar manner, red fluorescent Cys-modified maltose-containing Ag NCs ($\Phi = 3\%$) were synthesized by Basiruddin et al. and used in the detection of glycoprotein with HeLa cell labeling [117].

Apart from the detection of metal ions, anions, biomolecules, and proteins, templated Ag NCs were also well consumed for the identification of nucleic acid as mentioned below. DNA-templated Ag NCs were used in the detection of microRNA by Vosch and Ye's research groups using "turn-off" and "turn-on" responses, respectively [118,119]. Among them, the turn on response of DNA-Ag NCs to microRNA (miR-141) was seemingly more remarkable with an LOD of 2 aM (attomolar). In a similar response, DNA discoveries were established by Prof. Wang and Zhang's research reports with the utilization of DNA-Ag NCs [120,121]. In both cases, the linear ranges and LODs remain interesting. Hence, DNA-templated Ag NCs offers an efficient platform for detection of a wide spectrum of analytes.

As validated by Au NCs, templated Ag NCs are also being applied in bio-imaging and pH-sensing studies. The DNA-Ag NCs ($\Phi = 39.7\%$) were efficiently used in bio-imaging readings in HeLa cells by Zhu and co-workers [122]. Guével et al. reported the GSH-Ag NCs (Φ value of >60%) with blue-green, yellow, and red emissions, which was further used in bio-imaging of epithelial lung cancer cells (A549); hence, its application was proposed in biomolecular interaction diagnostics [123]. Qu et al. described the hyperbranched PEI-capped Ag NCs ($\Phi = 3.8\%$) as highly sensitive fluorescent and colorimetric pH sensors [124], in which, upon increasing acidity, the probe visualizes color changes from colorless to a colored state. On the other hand, fluorescence enhancement was observed at higher pH values. As a striking input to sensor research, He and Willner's research studies proved the uses of BSA-Ag NCs and DNA-Ag NCs for the detection of p-nitrophenol and nitroaromatic or RDX explosives, respectively [125,126]. Both investigations proved that the fluorescent-quenching responses and their LODs were in nano- and picomolar levels, correspondingly.

5. Sensor Applications of Cu NCs

Analogous to Au and Ag NCs, templated non-noble Cu NCs also acted as effective fluorescent probes and were regarded in various chemo- and biosensory studies as described in this section. They have also been used by researchers as attractive candidates for the determination of metal ions. For example, Prof. Huang and Mukherjee's research reports on Cu NCs witnessed its application in the detection of Fe³⁺ ions via fluorescent quenching [127,128]. To stabilize the Cu NCs, they used tannic acid and glutathione (GSH) as templates, respectively. Impressively, both Cu NCs exhibited blue emission with quantum yields of 14% and 6%, correspondingly. Furthermore, the detection of Fe³⁺ in both studies evidenced good linearity with LODs of 10 and 25 nM, individually. In this way, Liu et al. presented a hyperbranched PEI-protected copper nanoclusters (hPEI-Cu NCs; $\Phi = 7.9\%$) conjugated to the surface of silica-coated CdSe quantum dots (QDs) for the ratiometric detection of Cu²⁺ ions [129]. Here, the fluorescence of the probe drastically quenched between the linear range of 22 nM–8.8 μ M with an LOD of 8.9 nM.

Furthermore, glutathione (GSH)-capped Cu NCs ($\Phi = 10.6\%$) were applied as a fluorescent probe for sensitive and selective acknowledgement of Hg²⁺ in water and foodstuffs by Hu and co-workers [130]. In this work, upon the accumulation of Hg²⁺ ions, the fluorescence of GSH-Cu NCs

was quenched between the linear range from 10 nM to 10 μM with an LOD of 3.3 nM. Interestingly, the above probe with a quantum yield of 5.3% was also developed through sonochemical synthesis and consumed in fluorescent “turn-off” sensing of Pb^{2+} ions with an LOD of 1.0 nM [131]. On the other hand, Bing-Yan et al. represented the employment of GSH-Cu NCs in fluorescent “turn-on” recognition of Pb^{2+} ions [132]. However, the linear concentration of Pb^{2+} was lies between 200–700 μM , with an LOD of 106 μM . In this course, Goswami and co-workers represented the BSA-capped Cu NCs (CuQC@BSA) towards the selective fluorescent “on-off” detection of Pb^{2+} ions [133]. Here, the probe has a quantum yield of 0.15 and evidenced the aggregation-induced quenching with Pb^{2+} ions in the presence of other interferences. The development of diverse fluorescent Cu NCs toward sensory application is a more exciting concept. In this context, Prof. Huang’s research group attested dithiothreitol (DTT)-capped Cu NCs (DTT-Cu NCs) with orange fluorescence for the determination of Al^{3+} ions [134]. The detection mechanism was based on the aggregation-induced fluorescence enhancement with Al^{3+} ions. Notably, the linear relationship of DTT-Cu NCs with Al^{3+} ranged from 0.01 μM to 7 μM with an LOD of 0.01 μM . Similar to the above report, based on the aggregation-induced emission enhancement, Zn^{2+} ion discovery was proposed by GSH-Cu NCs ($\Phi = 1.3\%$) [135] as illustrated in Figure 10. This work was also proven through cellular imaging studies. Further, the detection range of Zn^{2+} was found to be from 4.68 μM to 2240 μM with an LOD of 1.17 μM . During Zn^{2+} determination, the Φ value increased to 6%.

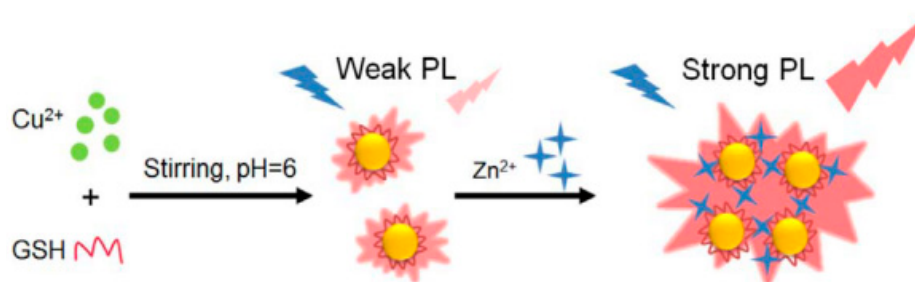


Figure 10. Schematic illustration of the preparation of GSH-capped Cu NCs and the aggregation induced PL enhancement of Cu NCs in the presence of Zn^{2+} (Copyright Ref [135], Elsevier publications).

Similar to metal ion sensors, precursor-stabilized Cu NCs were successfully used in the sensory investigation of anions as follows. Li et al. showed the fluorescent “turn-off” detection of S^{2-} ions by using cysteine-capped Cu NCs (Cys-Cu NCs) with real time applications in “Fart Bomb” samples [136]. The probe proposed the linear range from 0.2 μM to 50 μM with an LOD of 42 nM. Khonkayan et al. reported an impressive work for determination of CrO_4^{2-} by 4,6-diamino-2-mercaptopyrimidine-protected Cu NCs (DAMP-Cu NCs) [137]. Under optimized conditions, DAMP-Cu NCs has a linear response between the chromate concentration range of 1–7 μM with an LOD of 0.31 μM . In a similar response, PEI-templated copper nanoclusters (Cu NCs) have been used in the recognition of I^- ions between 0 μM and 10 μM linear range with an LOD of 100 nM [138]. Impressively, the obtained results were validated by urine sample analysis.

A contribution to anion sensor, stabilizer-free Cu NCs was made in the detection of NO_2^- ions by Qiu and co-workers [139] as illustrated in Figure 11. The probe witnessed the linear ranges varying from 12.5 nM to 125 μM and from 125 μM to 5000 μM with an LOD of 3.6 nM. Zhou et al. presented the GSH-Cu NCs ($\Phi = 8.6\%$) as the sensory probe for NO_2^- ions between the range of 1–100 mM, with an LOD of 0.3 μM [140]. Moreover, it was applied in real water sample investigations. Instead, thiosalicylic acid-capped Cu NCs with a quantum yield of 13.2% were engaged in the pH-dependent fluorescent “on-off” determination of NO_2^- and CN^- ions in water samples [141]. In which, at pH 5.0 and 8.0, the probe approximately quantify the NO_2^- and CN^- ions with limits of 5 μM and 5 nM, respectively. In contrast to other anion sensor reports by Cu NCs, Prof. Huang’s research group developed the trypsin-stabilized Cu NCs ($\Phi = 1.1\%$) towards the “turn-on” detection of pyrophosphate (PPi) with an

LOD of 101 nM [142]. Moreover, this probe also achieved good linear relationship between the PPI concentration range of 78 μM –20 mM.

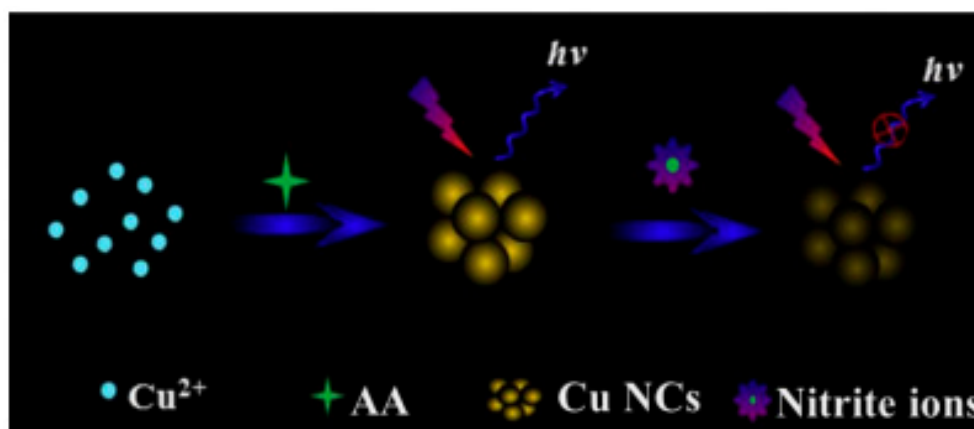


Figure 11. Schematic diagram of the mechanism of the detection of nitrite ions by the FL Cu NCs (Copyright Ref [139], Elsevier publications).

Similar to metal ions and anions sensors, scaffold-stabilized Cu NCs were also efficiently utilized in the detection of biomolecules, such as biothiols, cysteine, and glucose. For example, Hu et al. presented the DNA-Cu NCs based recognition of biothiols, such as GSH, Cys, and homocysteine (Hcy) via fluorescent-quenching responses [143] with affordable ranges and limits. Notably, this work was also applied in plasma samples. On the other hand, BSA-templated Cu NCs were used as peroxidase mimetics for the identification of H_2O_2 and glucose [144]. As shown in Figure 12, the addition of 2 mM glucose resulted in a bluer color than that of 5 mM fructose, lactose, or maltose.

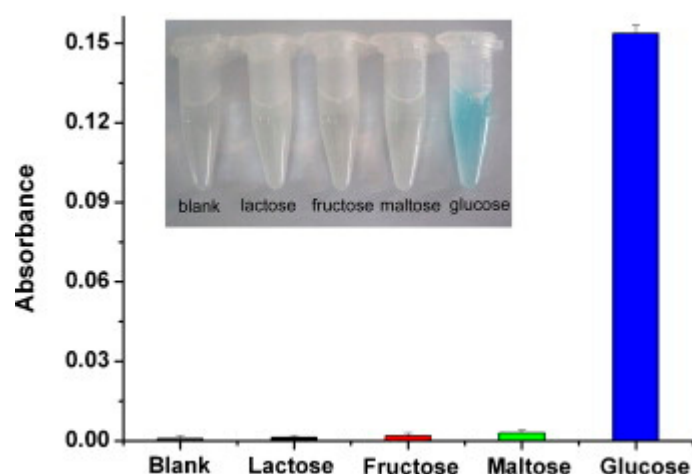


Figure 12. Determination of the selectivity of glucose detection with 5 mM lactose, 5 mM fructose, 5 mM maltose, and 2 mM glucose. The error bars represent the standard deviation of three measurements. Inset: the color change with the different solutions (Copyright Ref [144], ELSEVIER publications).

Added to this research, a guanosine 5'-triphosphate (GTP) sensor has been delivered by using histidine-protected Cu NCs with a quantum yield of 1.6% [145]. Zhao et al. presented an impressive work for the detection of GTP by fluorescence quenching response. However, other nucleoside triphosphates including adenosine-5'-triphosphate (ATP), CTP, UTP, and other inorganic anions, such as $\text{P}_2\text{O}_7^{4-}$, PO_4^{3-} , and CH_3COO^- , have no such effect on Cu NC emission. By contrast, Wang and co-workers accounted the DNA-templated Cu NCs in lieu of the assay of ATP via target-induced

structure-switching design [146]. This assay method showed an exciting fluorescence “turn-on” response compared with that of other non-specific nucleosides, such as CTP, UTP, and GTP. Moreover, this probe witnessed a dynamic assay range from 0.01 nM to 100 nM with an LOD of 5 pM.

In biomolecule detection, the lysozyme functionalized fluorescent copper nanoclusters (Lys-Cu NCs; $\Phi = 5.6\%$)-based glucose sensor via fluorescence quenching effect was reported by Wang et al. [147]. Lys-Cu NCs displayed the two linear response ranges with glucose between 0.03–10 μM and 0.5–10 mM with an LOD of 1.9 nM. In this course, fluorimetric sensing of Cys through the formation of various copper nanoclusters (Cys-Cu NCs) with different sizes were described [148]. As shown in Figure 13, in contrast to other amino acids, addition of Cu^{2+} to Cys solution leads to production of Cys-Cu NCs, and the fluorescence intensity increased with the accumulation of cysteine from 5 μM to 50 μM . In the presence of various concentrations of Cys, two linear ranges were observed between 5 μM to 50 μM and 60 μM to 500 μM with LOD values of 2.4 μM and 55 μM , separately.

The sensory studies of templated Cu NCs have been extended to detection of glycoproteins as noted next. For instance, BSA-Cu NCs were further functionalized by 3-aminophenylboronic acid and consumed in the sensitive detection of glycoproteins [149] via a fluorescence quenching response. The probe APBA-Cu NCs displayed a wide linear range of 5–220 nM and an LOD of 2.6 nM. Moreover, Li et al. successfully exploited this method for the determination of glycoproteins in the egg white of chickens and human urine samples, which shows quantitative spike recoveries from 95% to 104%. Zhao and co-workers described 4-methylthiophenol functionalized Cu NCs with a quantum yield of 2.4% in ethanol as an aggregation-induced emission probe and also consumed in β -galactosidase activity assay [150] by fluorescence “turn-off” response.



Figure 13. The effect of different amino acids on copper sulfate solution (pH = 12). From left to right: with Cys, Val, Gln, Ala, Lys, Met, Glu, Thr, Asn, Asp, Gly, Ser, Leu, Pro, Ile, Phe, Arg, Tyr, His, Trp, respectively (Copyright Ref [148], Springer publications).

Related to the nanoclusters of Au and Ag, Cu NCs with double-strand DNA (dsDNA) scaffold were also used in the recognition of microRNAs as defined next. Wang et al. presented DNA-Cu NCs for the quantitative detection of microRNAs via emission “turn-off” response [151]. Further, this work demonstrated the linear range from 1 pM to 10 nM with an LOD of 1 pM. By contrast, Prof. Hosseini described the DNA-Cu NC-based “turn-on” recognition of microRNA-155 [152]. In which, DNA-Cu NCs witnessed linear fluorescent enhancement towards miRNA-155 between 50 pM to 10 nM, with an LOD value of 11 pM. This method was also applied in human plasma and saliva.

Next, Cu NCs were meritoriously applied in bio-imaging studies as noted below. In this study, artificial peptide CLEDNN-templated Cu NCs with $\Phi = 7.3\%$ were used in bio-imaging and temperature-sensing applications by Huang et al. [153]. Basu and co-workers also presented GSH-stabilized multi-color emissive Cu NCs ($\Phi = 0.438$ – 1.27%) for bio-imaging investigations [154]. Here, copper nanoclusters countersigned with four different color emissions, such as blue, cyan, green, and orange-red, in water, which displayed low toxicity with imaging in OAW42 cell lines. Notably, Cu NCs were also used as pH sensors as in the case of other nanoclusters. For example,

Wang et al. described the trypsin-stabilized fluorescent Cu NCs ($\Phi = 1.1\%$) as a reversible pH sensor [155] between pH values 2.02–12.14. In this work, the Cu NCs form a blue precipitate in alkaline medium, which is restored upon dissolution in acid medium. Similar to the above report, Zhang et al. attested the reversible fluorescent pH-sensing ability of natural silk fibroin-capped Cu NCs (SF@Cu NCs) [156]. The author applied this method in water samples and demonstrated its potential practical application.

In addition to various sensor interrogations, Cu NCs were found to have potential in the detection of explosive materials. Prof. Wu's research paper indicated explosive determination by using BSA-Cu NCs [157]. The probe determined the 2,4,6-trinitrophenol via fluorescent "turn-off" and had linearity between $0.8 \mu\text{mol}\cdot\text{L}^{-1}$ to $100 \mu\text{mol}\cdot\text{L}^{-1}$ with an LOD of $20 \text{ nmol}\cdot\text{L}^{-1}$. In this method, Rogach and co-workers established the sensor efficacy of GSH-Cu NC incorporation in metal-organic frameworks (ZIF-8) towards the recognition of 2,4,6-trinitrotoluene by emission quenching [158]. Interestingly, Cu NCs were reported as probes for the identification of water in organic solvents at ultralow level (ppm) [159]. Moreover, the aggregation-induced emission enhancement capability of Cu NCs may lead to various future sensor applications [160].

6. Pt NCs in Sensory and Bio-Imaging Studies

Given the importance of nanocluster-based fluorescent sensors, fluorescent Pt NCs were developed, and currently, many research discoveries are being reported. Previously, Prof. Zhang proposed that a nonmetallic platinum nanocluster was responsible for the observed fluorescence behavior [161]. However, the fluorescent property of Pt NCs was found to be responsible for its sensor interrogations. For example, George and co-workers reported the utilization of dimethylformamide-protected Pt NCs as a fluorescent sensor towards Fe(III) ions in aqueous medium [162]. The probe displayed fluorescent "turn-off" selectivity to Fe(III) ions with impressive human blood sample analysis. In contrast to metal ion sensor, BSA-Pt NCs were used in the hypochlorite assay by fluorescent quenching [163] and oxidation mechanism. Given the negligible effect of other interferences, this method was validated as highly selective.

In the detection of biologically important species, Jin and Shang co-workers represented the ultra-small Pt NCs ($\Phi = 8.4\%$) as robust peroxidase mimics for colorimetric recognition of glucose in human serum [164]. This work revealed the Stern–Volmer plot with good linear relationship from $0 \mu\text{M}$ to $200 \mu\text{M}$ with an LOD of $0.28 \mu\text{M}$. Moreover, upon addition of glucose, the blue color was visualized more than that of other carbohydrates (lactose, fructose, sucrose, and maltose) at higher concentration. Xu et al. described the hydrothermal synthesis of highly luminescent polyethylenimine-protected Pt NCs (Pt NCs@PEI; $\Phi = 28\%$) and applied it in the recognition of nitroimidazoles [165]. Pt NCs@PEI effectively determined trace amount of metronidazole (MTZ), used in treating parasitic infections, at a linear response between $0.25 \mu\text{M}$ to $300 \mu\text{M}$ with an LOD of $0.1 \mu\text{M}$.

Pt NCs have also been used considerably in cellular imaging practices. For instance, Chen and co-workers validated Pt NC-based bio-imaging and photothermal treatment [166,167]. They united the spontaneous intracellular creation of fluorescent Pt NCs with a photothermal treatment of tumors through water-soluble porphyrin tetrakis(sulfonatophenyl)porphyrin, leading to synergistic effects and enhancement of the therapeutic efficacy of IR irradiation [167], as illustrated in Figure 14.

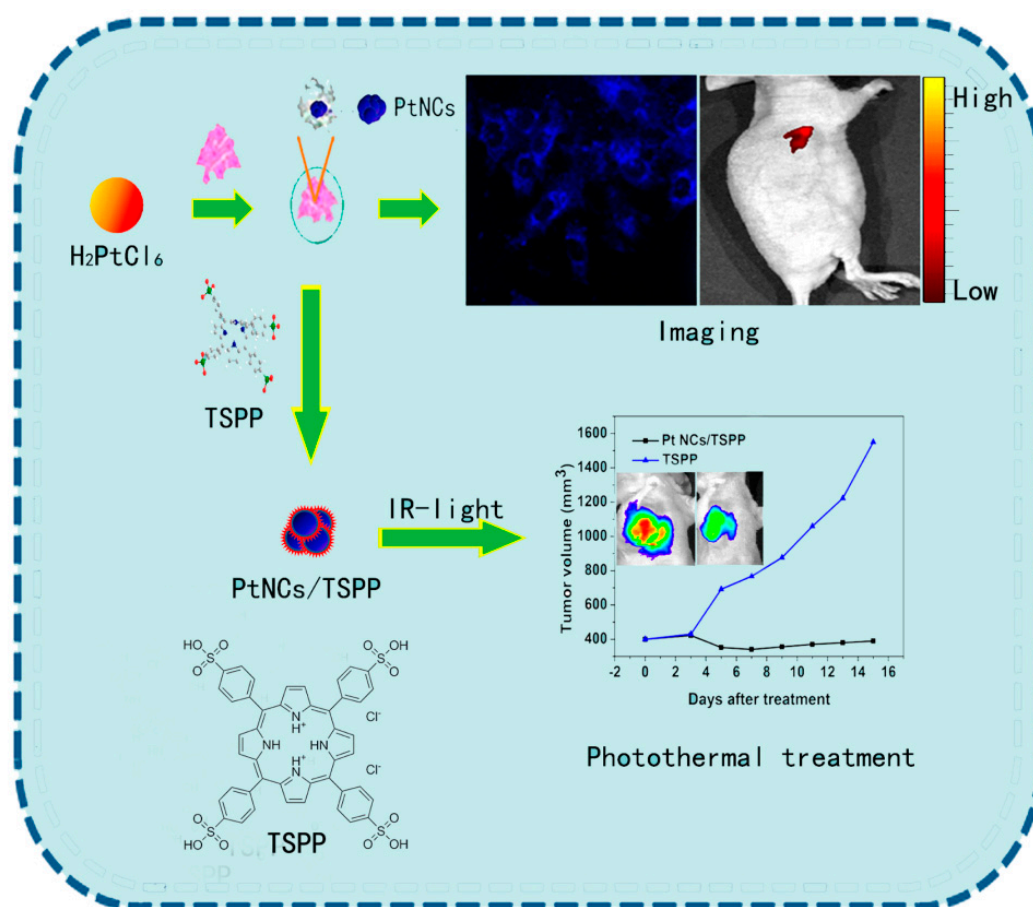


Figure 14. Schematic illustration of the study rationale and design (Copyright Ref [167], American Chemical Society).

7. Other Metal Nanoclusters as Sensors

The nanoclusters of Au, Ag, Cu, Pt, and currently other metal nanocluster-based sensory are becoming interesting topics. Very excitingly, those M-NCs may also be applied in sensory and imaging studies as noted subsequently. In this direction, King et al. pronounced the plasmonic colorimetric sensor ability of aluminum nanoclusters (Al NCs) [168], which may lead to the development of Al NC-based sensors for visual readout of a variety of analytes. As an addition to this research, palladium nanoclusters (Pd NCs) were established by Prof. Atta in the past decade [169]. Pd NC-coated polyfuran was used as a sensor probe for the determination of catecholamine neurotransmitters and paracetamol. However, this work applied electrochemical investigations not fluorescent studies, and hence, cannot be attested to our current focus. The uses of metal nanoclusters of Cd and Ir were also validated in cellular imaging studies [170,171]. Sarparast et al. represented such Cd NCs in a protein matrix, which were applied in targeted drug delivery and cellular imaging [170]. In a similar fashion, Vankayala and co-workers recognized the cellular imaging practice of highly fluorescent and biocompatible Ir NCs with a quantum yield of 0.36% [171]. Notably, the development of fluorescent nanoclusters, other than Au, Ag, Cu, and Pt still requires more focus to improve their practicability. Hence, many scientists are working on these research investigations.

8. Bi-Metallic Nanoclusters in Sensors and Bio-Imaging

Given the improved stability and optical properties, research on bi-metallic NCs have gained increasing attention. Notably, many reports on bi-metallic NCs are still more operative towards sensory, bio-imaging and drug delivery. Therefore, in this section, we intend to deliver a few examples of

sensory and bio-imaging applications of bi-metallic NCs. In the last decade, Su et al. conveyed the sensor utility of DNA-templated copper/silver nanoclusters (DNA-Cu/Ag NCs) in the presence of mercaptopropionic acid (MPA) for the determination of Cu^{2+} ions via fluorescence recovery [172]. Here, in the presence of MPA, the fluorescence of DNA-Cu/Ag NCs was quenched and then recovered during the addition of Cu^{2+} ions. The linear concentration range of Cu^{2+} ions was established as 0–0.2 μM with an LOD of 2.7 nM. Next, mercaptosuccinic acid-stabilized AgAu alloy nanoclusters (MSA-AgAu NCs) with highly red fluorescence were developed by Prof. Chen's research group and applied in the fluorescence-enhanced detection of Al^{3+} ions [173]. In this work, the linear Al^{3+} concentration lies between 2.0–30 μM with an LOD of 0.8 μM .

As mentioned earlier, the templated Ag/Au NCs became more attractive by tuning the atomic ratio. Moreover, among other bi-metallic systems, the Ag/Au system provides more stability with enhanced fluorescence and biocompatibility for sensory and imaging studies. Some metal ion sensor-based Ag/Au bi-metallic NCs are as follows. Zhang et al. established the Au/Ag NCs in the protein matrix with "Silver Effect"-enhanced red fluorescence [174]. Importantly, the above-mentioned probe Au-Ag NCs facilitated the recognition of Hg^{2+} and Cu^{2+} ions with corresponding LODs of 0.30 and 0.60 nM in blood samples. Continuing, Zheng and co-workers described the (BSA)-stabilized yellow emissive AuAg bimetallic nanoclusters as a sensory probe for Hg^{2+} ions by "turn-off" response [175]. The linear detection concentration of Hg^{2+} ions was established as 50 nM to 63 μM with an LOD value of 13 nM. In this way, lipoic acid-protected red emissive Au/Ag nanoclusters with a quantum yield of 6.4% were applied as a probe for the determination of Fe^{3+} ions and temperature through fluorescence quenching [176]. The above probe was developed by Prof. Wang's research unit via one-step green synthesis and has linear reversible response to temperatures between 20 °C and 65 °C. Furthermore, linear fluorescent-quenching responses of Au/Ag nanoclusters with Fe^{3+} ions were observed between 1–80 μM with an LOD value of 0.5 μM . The sensor ability of the probe was also validated through cellular imaging studies.

AuAg NCs with diverse templates were also reported for the detection of different metal ions as noted next. Yang et al. described the 11-mercaptopundecanoic acid (11-MUA)-capped AuAg NCs, which show significant fluorescence quenching in the presence of Cr(III) ions [177]. However, the probe participated in the redox reaction (between Cr(VI) and AA) for indirect discovery of Cr(VI) ions. The above interrogation estimated the linear ranges of Cr(III) and Cr(VI) as 0.08 μM to 6 μM and 0.6 μM to 10 μM , respectively, with matching LOD values of 0.05 and 0.3 μM . In a similar trend, DNA-scaffolded Ag-Au NCs were expended in the selective recognition of Hg^{2+} ions through fluorescence quenching [178]. Similar to Ag-Au NCs, other bi-metallic NCs were also consumed in analyte detection. Ding et al. presented dual-emitting BSA-Pt-Au NCs in the detection of mercury ions and cysteine via ratiometric fluorescence responses [179]. In this result, upon addition of metal ions, the BSA-Pt-Au NCs exhibited emission quenching and then recovered in the presence of Cys. The linear concentration range of Hg^{2+} and Cys was observed between 0.5 nM to 22 μM and 0.1 μM to 50 μM with LODs of 0.3 nM and 0.04 μM , respectively. Wang and co-workers described the fluorometric determination of Cd(II) and Hg(II) ions by using gold-nickel bi-metallic NCs [180]. The fluorescence signal was strongly enhanced in the presence of Cd(II) ions but quenched upon addition of Hg(II) ions via a diverse electron transfer mechanism (Figure 15). This probe witnessed a good linear relationship with Cd(II) ions from 0.005 μM to 100 μM with an LOD of 1.75 nM. On the other hand, the linear relationship for Hg(II) ions was appraised as 0.005–1.0 μM with an LOD value of 1.70 nM. Moreover, the above work was also authenticated by serum sample analysis.

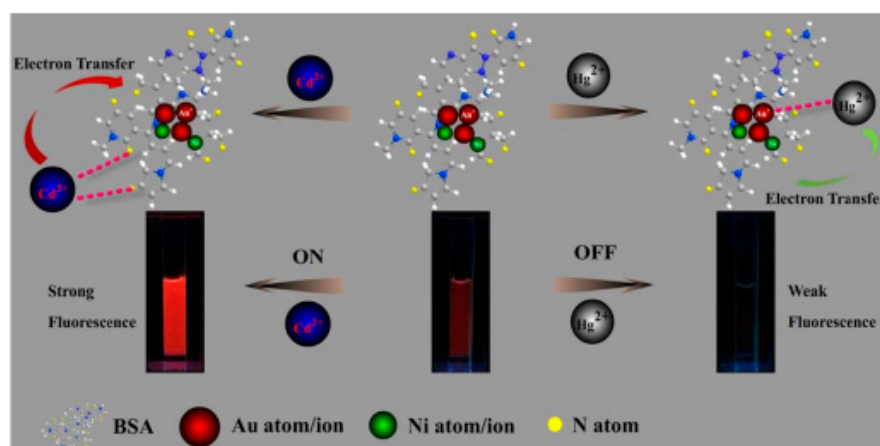


Figure 15. Schematic diagram of the mechanism of the detection of Cd^{2+} and Hg^{2+} ions by the fluorescent BSA-Au-Ni NCs (Copyright Ref [180], Springer publications).

Comparable with the detection of metal ions, bi-metallic NCs were also used in the selective acknowledgement of anions as revealed successively. Prof. Chang's research study exposed the effective utility of DNA-templated gold/silver nanoclusters ($\Phi = 3.9\%$) in the assay of S^{2-} ions [181] with an LOD of 0.83 nM via fluorescent "turn-off" response. In a related fluorescence response, the detection of hypochlorite in tap water was exposed by BSA-stabilized Au-Ag NCs ($\Phi = 18.6\%$) [182], in which the linearly correlated hypochlorite concentration ranged from 0.7 μM to 15 μM with an LOD of 80 nM. A similar probe (BSA-Au-Ag NCs) was also used by Zhou et al. for the highly sensitive recognition of inorganic pyrophosphatase activity with the help of copper ion (Cu^{2+}) and inorganic pyrophosphate ion (PPi), as illustrated in Figure 16 [183].

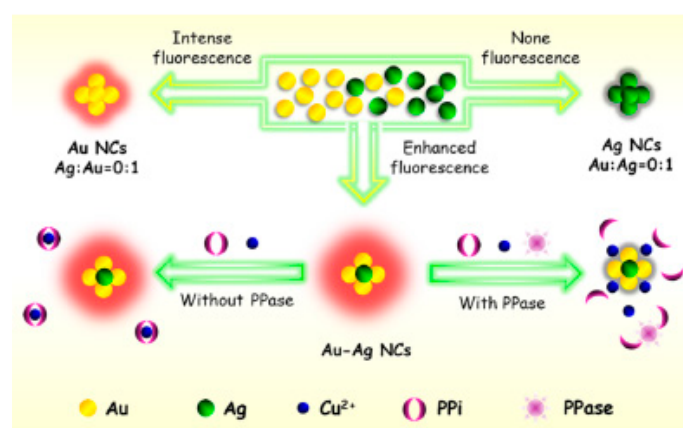


Figure 16. Schematic illustration of gold-silver bimetallic nanocluster (Au-Ag NCs) based fluorescent probes for quantitative monitoring of inorganic pyrophosphatase (PPase) activity coupling enzyme-induced hydrolysis of pyrophosphate ion (PPi, $\text{P}_2\text{O}_7^{4-}$) with the release of copper ion (Cu^{2+}) from the Cu^{2+} -PPi complexes (Copyright Ref [183], American Chemical Society).

Li et al. approved the sensor ability of DNA-capped Au/Ag NCs in the fluorometric and colorimetric determination of I^- ions by fluorescence quenching [184]. Here, the probe showed a good linear range from 0 $\mu\text{mol}\cdot\text{L}^{-1}$ to 10 $\mu\text{mol}\cdot\text{L}^{-1}$ for iodide ions with an LOD of 0.3 $\mu\text{mol}\cdot\text{L}^{-1}$. Alternatively, Ding et al. applied the DNA-templated copper/silver nanoclusters (DNA-Cu/AgNCs) for selective sensing of S^{2-} ions via emission quenching [185]. DNA-Cu/AgNCs displayed a linear detection range of S^{2-} between 10 pM to 1 mM with an LOD of 3.75 pM. Moreover, it was successfully applied in the detection of H_2S in poisoning blood.

Given the importance of biomolecule determination, bi-metallic NCs were also consumed for their fluorescent sensor recognition as subsequently defined. For instance, Wang et al. reported the detection of biologically important thiols, such as Cys and GSH via fluorescence quenching of BSA-Au/Ag NCs [186]. Under optimized conditions, the above probe has excellent linear fluorescence quenching in the presence of Cys (20 nM–80 μ M, LOD: 5.87 nM) and GSH (2–70 μ M, LOD: 1.01 μ M). By contrast, fluorescence turn-on selective identification of His and Cys were discovered by Sun and co-workers using 11-mercaptoundecanoic acid (11-MUA) protected Ag/Au bimetallic nanoclusters ($\Phi = 4.2\%$) combined with Cu^{2+} ions [187]. The probe can detect His and Cys within the linear concentration range of 0.25–9 μ M and 0.25–7 μ M with LODs of 87 nM and 111 nM, correspondingly.

Prof. Wu's research legitimated the fabrication of gold–platinum bimetallic nanoclusters (Au-Pt NCs) with variable Au/Pt molar ratios via a one-pot synthetic route and applied in colorimetric acknowledgement of glucose [188]. Here, Au-Pt NCs led to a glucose oxidase cascade-catalyzed system using 3,3',5,5'-tetramethylbenzidine as a chromogenic substrate. This convenient naked eye quantification has linear responses between 5 μ M to 55 μ M with an LOD value of 2.4 μ M. Moreover, upon incremental addition of glucose, the absorption spectra seem to be enhanced at 652 nm along with blue color visualization by the naked eye (Figure 17).

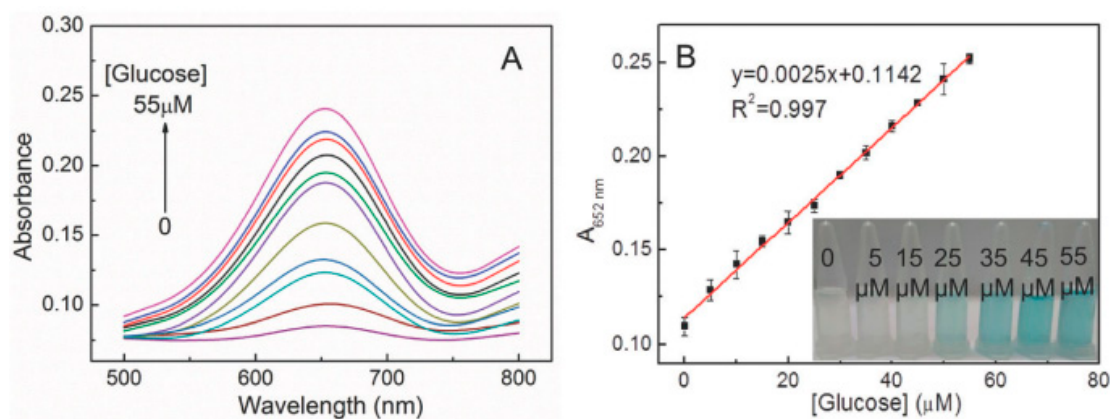


Figure 17. (A) Absorption spectra of the Au-Pt NCs-GOx-TMB system in the presence of different glucose concentrations (0, 5, 10, 15, 20, 25, 30, 35, 40, 45, 50, and 55 μ M). (B) Linear calibration curve of the absorbance at 652 nm against glucose concentration. The inset shows the corresponding photographs for different concentrations of glucose (Copyright Ref [188], Royal Society of Chemistry).

Ahn et al. presented the detection of adenosine by consuming DNA-templated Cu/Ag NCs and using the *s*-adenosylhomocysteine hydrolase method [189]. The adenosine was detected between 0 and 1 μ M with an LOD of 19 nM more than that of other analogs, such as AMP, ADP, ATP, cAMP, guanosine, cytidine, and urine. Moreover, this method was also well verified with real human serum sample studies. In addition to this research, Li et al. marked the cost-effective highly sensitive fluorometric assay of acetylcholinesterase (AChE-significant neural enzyme), which can specifically catalyze the hydrolysis of acetylcholine (ACh—a central neurotransmitter), to acetic acid and choline [190]. Similar to individual M-NCs, hybrid bi-metallic NCs were also used in cellular imaging investigations as follows.

Previously, Hu et al. reported the hybrid ultra-small Au/Gd-NCs in triple-modal NIRF/CT/MRI imaging [191]. This work demonstrates the penetration of Au/Gd NCs into a solid tumor without any toxicity *in vivo*. In a similar fashion, BSA-stabilized Au-Ag NCs ($\Phi = 11.7\%$) were established for the delivery of the therapeutic suicide gene in HeLa cancer cells by Dutta and co-workers [192]. The above study described the mechanism of uptake and manner of cell death and revealed its future applicability. In this trend, bright fluorescent cytidine-mediated Au-Ag NCs were developed by Chen et al. and utilized for both *in vitro* cellular imaging and tumor *in vivo* detection [193]. The synthesis and tumor detective application of the above-acknowledged probe is shown in Figure 18.

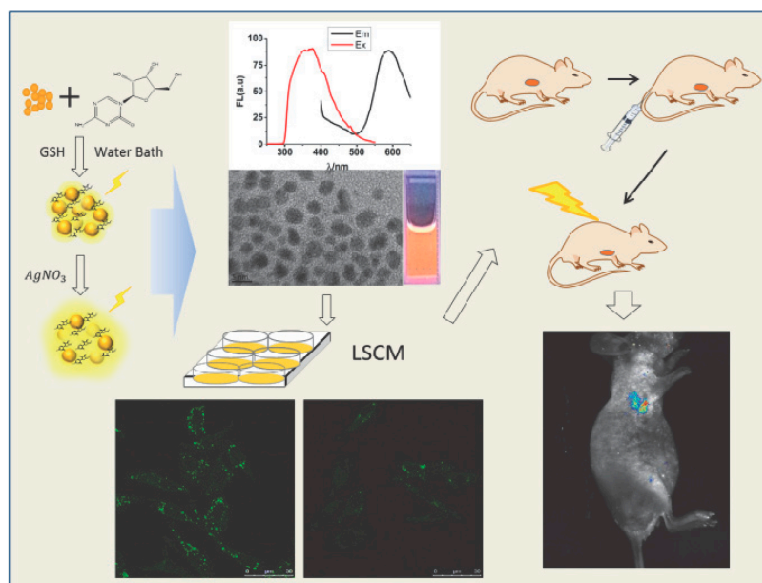


Figure 18. Scheme illustration of the process for cytidine mediated gold-silver nanoclusters (AuAg NCs) (Copyright Ref [193], WILEY publications).

As in the case of other individual NCs, bi-metallic NCs were used in pH and temperature sensor applications. For example, Prof. Chang's research paper defined the pH sensing ability of AuCu bimetallic NCs ($\Phi = 4.8\%$), which was synthesized through a one-pot approach [194]. Notably, the above probe also showed the catalytic activity in the degradation of methylene blue. Han et al. represented the temperature-sensing capability of Cu/Ag NCs obtained from weakly luminescent glutathione (GSH)-capped Cu NCs [195]. Cu/Ag NCs witnessed fluorescence quenching between 4 °C and 55 °C. Further to note, the aggregation-induced behavior of M-NCs and bi-MNCs were evaluated and may be applied in many biological applications in the near future [196]. Attracted by the effective applications of M-NCs and bi-MNCs, researchers currently intend to develop luminescent tri-metallic NCs with high quantum yields [197].

9. Advantages and Limitations

NC-based sensory investigations have several advantages and a few limitations as indicated below.

1. In contrast to plasmonic nanoparticles, M-NCs have an ultra-small size with ultimate fluorescence. Hence, they can be used as fluorescent "Off" or "On" probes in a variety of analytical studies.
2. Contrary to fluorescent quantum dots, the optical properties of M-NCs can be enhanced by controlling the surface functionalization, which also leads to NCs with diverse emissive colors.
3. M-NCs can be synthesized via a one-pot synthesis compared with the complicated synthesis of organic sensory probes.
4. Luminescent M-NCs exhibit less toxicity and good biocompatibility compared with fluorescent quantum dots and organic fluorophores. Hence, they can be used in biological applications, such as imaging and drug delivery studies.
5. The emissive characteristics of M-NCs are limited to the ligands functionalized on the surface and to stability with respect to temperature, time, and pH values.
6. The optical properties are also limited to overall uniform cluster particle sizes. Similar functional groups on the NC surface with diverse particle sizes may also possibly emit different colors. Therefore, maintenance of the experimental procedure is highly essential to obtain reproducible results.

10. Conclusions and Perspectives

In this review, we have summarized the recent progress in chemosensory applications of luminescent metal NCs with particular focus on Au, Ag, Cu, Pt, and their alloy clusters. These NCs remain more attractive due to their diverse color emission properties by tuning the templates or metal ratios. Interestingly, they act as probes in specific analyte detection, such as metal ions, anions, biomolecules, peptides/proteins, and explosives. Moreover, due to their low toxicity and biocompatibility, they are also used in bio-imaging studies. Hence, in the presence of biofunctionalized scaffolds, the ultra-small metal NCs can be utilized in a variety of biomedical applications. The unique fluorescent property of those NCs enhances the reversible pH and temperature-sensing ability.

Although the M-NCs and bi-NCs have witnessed exciting progress, many limitations remain as a challenge.

1. The relation between structure and emission properties of many reported M-NCs remains insufficient. Hence, fundamental investigations on the structural properties of M-NCs need to be focused along with fluorescence studies.
2. Optimization of precursor/template concentration for stabilizing the M-NCs has been uncertain in many cases and must be clarified. Notably, in many reports, similar probes with various template or metal ion concentrations have been reported for diverse analyte detection. However, clear fundamental evidence to support their diverse optical properties has not been provided. This is an essential point to be addressed in future reports.
3. Mechanistic evidence for a few M-NC-based sensory reports remain inadequate. Hence, essential theoretical interrogations should be supplemented in the future.
4. NC-based sensory applications by using optical devices have led them towards promising nanodevice-based commercial utilities.
5. Pt NCs based sensory research remains insufficient, with emitted fluorescence between 700 nm to 950 nm by utilization of diverse templates. Hence, much effort is needed to develop such probes for enhanced biological utilities.
6. The development of multifunctional M-NCs is helpful in biomedical diagnosis and treatment. Hence, considerable efforts are required to develop promising candidates.

Apart from the above-mentioned challenges, the research on M-NCs and bi-MNCs remains promising for sensory and biomedical applications. Further, many scientists continue to resolve many of the above issues, and hence, it is believed that NC-based sensory and theranostic applications should have a bright future.

Conflicts of Interest: The authors declare no conflict of interest.

References

1. Chakraborty, I.; Pradeep, T. Atomically Precise Clusters of Noble Metals: Emerging Link between Atoms and Nanoparticles. *Chem. Rev.* **2017**, *117*, 8208–8271. [[CrossRef](#)] [[PubMed](#)]
2. Song, X.-R.; Goswami, N.; Yang, H.-H.; Xie, J. Functionalization of metal nanoclusters for biomedical applications. *Analyst* **2016**, *141*, 3126–3140. [[CrossRef](#)] [[PubMed](#)]
3. Sun, H.-T.; Yoshio, S. Luminescent metal nanoclusters: Controlled synthesis and functional applications. *Sci. Technol. Adv. Mater.* **2014**, *15*, 014205. [[CrossRef](#)] [[PubMed](#)]
4. Zhao, T.; Zhou, T.; Yao, Q.; Hao, C.; Chen, X. Metal Nanoclusters: Applications in Environmental Monitoring and Cancer Therapy. *J. Environ. Sci. Health C* **2015**, *33*, 168–187. [[CrossRef](#)] [[PubMed](#)]
5. Santiago-Gonzalez, B.; Monguzzi, A.; Caputo, M.; Villa, C.; Prato, M.; Santambrogio, C.; Torrente, Y.; Meinardi, F.; Brovelli, S. Metal Nanoclusters with Synergistically Engineered Optical and Buffering Activity of Intracellular Reactive Oxygen Species by Compositional and Supramolecular Design. *Sci. Rep.* **2017**, *7*, 5976. [[CrossRef](#)] [[PubMed](#)]

6. Tao, Y.; Li, M.; Ren, J.; Qu, X. Metal nanoclusters: Novel probes for diagnostic and therapeutic applications. *Chem. Soc. Rev.* **2015**, *44*, 8636–8663. [[CrossRef](#)] [[PubMed](#)]
7. Wilcoxon, J.P.; Abrams, B.L. Synthesis, structure and properties of metal nanoclusters. *Chem. Soc. Rev.* **2006**, *35*, 1162–1194. [[CrossRef](#)] [[PubMed](#)]
8. Yu, P.; Wen, X.; Toh, Y.-R.; Ma, X.; Tang, J. Fluorescent Metallic Nanoclusters: Electron Dynamics, Structure, and Applications. *Part. Part. Syst. Charact.* **2015**, *32*, 142–163. [[CrossRef](#)]
9. Zhang, L.; Wang, E. Metal nanoclusters: New fluorescent probes for sensors and bioimaging. *Nano Today* **2014**, *9*, 132–157. [[CrossRef](#)]
10. Lu, Y.; Chen, W. Sub-nanometre sized metal clusters: From synthetic challenges to the unique property discoveries. *Chem. Soc. Rev.* **2012**, *41*, 3594–3623. [[CrossRef](#)] [[PubMed](#)]
11. Fang, J.; Zhang, B.; Yao, Q.; Yang, Y.; Xie, J.; Yan, N. Recent advances in the synthesis and catalytic applications of ligand-protected, atomically precise metal nanoclusters. *Coord. Chem. Rev.* **2016**, *322*, 1–29. [[CrossRef](#)]
12. Li, J.; Zhu, J.-J.; Xu, K. Fluorescent metal nanoclusters: From synthesis to applications. *TrAC Trends Anal. Chem.* **2014**, *58*, 90–98. [[CrossRef](#)]
13. Li, C.; Chen, H.; Chen, B.; Zhao, G. Highly fluorescent gold nanoclusters stabilized by food proteins: From preparation to application in detection of food contaminants and bioactive nutrients. *Crit. Rev. Food Sci. Nutr.* **2016**, 1–11. [[CrossRef](#)] [[PubMed](#)]
14. Li, M.; Gou, H.; Al-Ogaidi, I.; Wu, N. Nanostructured Sensors for Detection of Heavy Metals: A Review. *ACS Sustain. Chem. Eng.* **2013**, *1*, 713–723. [[CrossRef](#)]
15. Yuan, X.; Luo, Z.; Yu, Y.; Yao, Q.; Xie, J. Luminescent Noble Metal Nanoclusters as an Emerging Optical Probe for Sensor Development. *Chem. Asian J.* **2013**, *8*, 858–871. [[CrossRef](#)] [[PubMed](#)]
16. Chen, L.-Y.; Wang, C.-W.; Yuan, Z.; Chang, H.-T. Fluorescent Gold Nanoclusters: Recent Advances in Sensing and Imaging. *Anal. Chem.* **2015**, *87*, 216–229. [[CrossRef](#)] [[PubMed](#)]
17. Sun, J.; Jin, Y. Fluorescent Au nanoclusters: Recent progress and sensing applications. *J. Mater. Chem. C* **2014**, *2*, 8000–8011. [[CrossRef](#)]
18. Diez, I.; Ras, R.H.A. Fluorescent silver nanoclusters. *Nanoscale* **2011**, *3*, 1963–1970. [[CrossRef](#)] [[PubMed](#)]
19. Xu, H.; Suslick, K.S. Water-Soluble Fluorescent Silver Nanoclusters. *Adv. Mater.* **2010**, *22*, 1078–1082. [[CrossRef](#)] [[PubMed](#)]
20. Lu, Y.; Wei, W.; Chen, W. Copper nanoclusters: Synthesis, characterization and properties. *Chin. Sci. Bull.* **2012**, *57*, 41–47. [[CrossRef](#)]
21. Wang, Z.; Chen, B.; Rogach, A.L. Synthesis, optical properties and applications of light-emitting copper nanoclusters. *Nanoscale Horiz.* **2017**, *2*, 135–146. [[CrossRef](#)]
22. Chakraborty, I.; Bhuin, R.G.; Bhat, S.; Pradeep, T. Blue emitting undecaplatinum clusters. *Nanoscale* **2014**, *6*, 8561–8564. [[CrossRef](#)] [[PubMed](#)]
23. Tanaka, S.-I.; Aoki, K.; Muratsugu, A.; Ishitobi, H.; Jin, T.; Inouye, Y. Synthesis of green-emitting Pt₈ nanoclusters for biomedical imaging by pre-equilibrated Pt/PAMAM (G4-OH) and mild reduction. *Opt. Mater. Express* **2013**, *3*, 157–165. [[CrossRef](#)]
24. Sun, Y.; Wu, J.; Wang, C.; Zhao, Y.; Lin, Q. Tunable near-infrared fluorescent gold nanoclusters: Temperature sensor and targeted bioimaging. *New J. Chem.* **2017**, *41*, 5412–5419. [[CrossRef](#)]
25. Wang, Y.; Dai, C.; Yan, X.-P. Fabrication of folate bioconjugated near-infrared fluorescent silver nanoclusters for targeted in vitro and in vivo bioimaging. *Chem. Commun.* **2014**, *50*, 14341–14344. [[CrossRef](#)] [[PubMed](#)]
26. Wang, C.; Cheng, H.; Sun, Y.; Lin, Q.; Zhang, C. Rapid Sonochemical Synthesis of Luminescent and Paramagnetic Copper Nanoclusters for Bimodal Bioimaging. *ChemNanoMat* **2015**, *1*, 27–31. [[CrossRef](#)]
27. Tanaka, S.-I.; Miyazaki, J.; Tiwari, D.K.; Jin, T.; Inouye, Y. Fluorescent Platinum Nanoclusters: Synthesis, Purification, Characterization, and Application to Bioimaging. *Angew. Chem. Int. Ed.* **2011**, *50*, 431–435. [[CrossRef](#)] [[PubMed](#)]
28. Wang, Y.; Hu, L.; Li, L.; Zhu, J.-J. Fluorescent Gold Nanoclusters: Promising Fluorescent Probes for Sensors and Bioimaging. *J. Anal. Test.* **2017**, *1*, 13. [[CrossRef](#)]
29. Shang, L.; Dörlich, R.M.; Trouillet, V.; Bruns, M.; Ulrich Nienhaus, G. Ultrasmall fluorescent silver nanoclusters: Protein adsorption and its effects on cellular responses. *Nano Res.* **2012**, *5*, 531–542. [[CrossRef](#)]

30. Jia, X.; Li, J.; Wang, E. Cu Nanoclusters with Aggregation Induced Emission Enhancement. *Small* **2013**, *9*, 3873–3879. [[CrossRef](#)] [[PubMed](#)]
31. Huang, X.; Ishitobi, H.; Inouye, Y. Formation of fluorescent platinum nanoclusters using hyper-branched polyethylenimine and their conjugation to antibodies for bio-imaging. *RSC Adv.* **2016**, *6*, 9709–9716. [[CrossRef](#)]
32. Shang, L.; Dong, S.; Nienhaus, G.U. Ultra-small fluorescent metal nanoclusters: Synthesis and biological applications. *Nano Today* **2011**, *6*, 401–418. [[CrossRef](#)]
33. Yuan, X.; Dou, X.; Zheng, K.; Xie, J. Recent Advances in the Synthesis and Applications of Ultrasmall Bimetallic Nanoclusters. *Part. Part. Syst. Charact.* **2015**, *32*, 613–629. [[CrossRef](#)]
34. Cercis, M.-B.; Francisco, H.; Cecilia, N. On the stability of noble-metal nanoclusters protected with thiolate ligands. *Europhys. Lett.* **2017**, *119*, 56002.
35. Huang, C.-C.; Yang, Z.; Lee, K.-H.; Chang, H.-T. Synthesis of Highly Fluorescent Gold Nanoparticles for Sensing Mercury(II). *Angew. Chem. Int. Ed.* **2007**, *46*, 6824–6828. [[CrossRef](#)] [[PubMed](#)]
36. Goswami, N.; Lin, F.; Liu, Y.; Leong, D.T.; Xie, J. Highly Luminescent Thiolated Gold Nanoclusters Impregnated in Nanogel. *Chem. Mater.* **2016**, *28*, 4009–4016. [[CrossRef](#)]
37. Aldeek, F.; Muhammed, M.A.H.; Palui, G.; Zhan, N.; Mattoussi, H. Growth of Highly Fluorescent Polyethylene Glycol- and Zwitterion-Functionalized Gold Nanoclusters. *ACS Nano* **2013**, *7*, 2509–2521. [[CrossRef](#)] [[PubMed](#)]
38. Deng, H.-H.; Shi, X.-Q.; Wang, F.-F.; Peng, H.-P.; Liu, A.-L.; Xia, X.-H.; Chen, W. Fabrication of Water-Soluble, Green-Emitting Gold Nanoclusters with a 65% Photoluminescence Quantum Yield via Host–Guest Recognition. *Chem. Mater.* **2017**, *29*, 1362–1369. [[CrossRef](#)]
39. Muhammed, M.A.H.; Aldeek, F.; Palui, G.; Trapiella-Alfonso, L.; Mattoussi, H. Growth of In Situ Functionalized Luminescent Silver Nanoclusters by Direct Reduction and Size Focusing. *ACS Nano* **2012**, *6*, 8950–8961. [[CrossRef](#)] [[PubMed](#)]
40. Naaz, S.; Poddar, S.; Bayen, S.P.; Mondal, M.K.; Roy, D.; Mondal, S.K.; Chowdhury, P.; Saha, S.K. Tenfold enhancement of fluorescence quantum yield of water soluble silver nanoclusters for nano-molar level glucose sensing and precise determination of blood glucose level. *Sens. Actuators B* **2018**, *255*, 332–340. [[CrossRef](#)]
41. Ghosh, R.; Sahoo, A.K.; Ghosh, S.S.; Paul, A.; Chattopadhyay, A. Blue-Emitting Copper Nanoclusters Synthesized in the Presence of Lysozyme as Candidates for Cell Labeling. *ACS Appl. Mater. Interfaces* **2014**, *6*, 3822–3828. [[CrossRef](#)] [[PubMed](#)]
42. Wang, Z.; Chen, B.; Susha, A.S.; Wang, W.; Reckmeier, C.J.; Chen, R.; Zhong, H.; Rogach, A.L. All-Copper Nanocluster Based Down-Conversion White Light-Emitting Devices. *Adv. Sci.* **2016**, *3*, 1600182. [[CrossRef](#)] [[PubMed](#)]
43. Jenifer García, F.; Laura, T.-A.; José, M.C.-F.; Rosario, P.; Alfredo, S.-M. Aqueous synthesis of near-infrared highly fluorescent platinum nanoclusters. *Nanotechnology* **2015**, *26*, 215601. [[CrossRef](#)] [[PubMed](#)]
44. Jin, R. Atomically precise metal nanoclusters: Stable sizes and optical properties. *Nanoscale* **2015**, *7*, 1549–1565. [[CrossRef](#)] [[PubMed](#)]
45. Taylor, M.G.; Mpourmpakis, G. Thermodynamic stability of ligand-protected metal nanoclusters. *Nat. Commun.* **2017**, *8*, 15988. [[CrossRef](#)] [[PubMed](#)]
46. Goswami, N.; Luo, Z.; Yuan, X.; Leong, D.T.; Xie, J. Engineering gold-based radiosensitizers for cancer radiotherapy. *Mater. Horiz.* **2017**, *4*, 817–831. [[CrossRef](#)]
47. Yang, X.; Yang, L.; Dou, Y.; Zhu, S. Synthesis of highly fluorescent lysine-stabilized Au nanoclusters for sensitive and selective detection of Cu²⁺ ion. *J. Mater. Chem. C* **2013**, *1*, 6748–6751. [[CrossRef](#)]
48. Deng, H.-H.; Zhang, L.-N.; He, S.-B.; Liu, A.-L.; Li, G.-W.; Lin, X.-H.; Xia, X.-H.; Chen, W. Methionine-directed fabrication of gold nanoclusters with yellow fluorescent emission for Cu²⁺ sensing. *Biosens. Bioelectron.* **2015**, *65*, 397–403. [[CrossRef](#)] [[PubMed](#)]
49. Wu, J.; Jiang, K.; Wang, X.; Wang, C.; Zhang, C. On–off–on gold nanocluster-based near infrared fluorescent probe for recognition of Cu(II) and vitamin C. *Microchim. Acta* **2017**, *184*, 1315–1324. [[CrossRef](#)]
50. Liu, P.; Shang, L.; Li, H.; Cui, Y.; Qin, Y.; Wu, Y.; Hiltunen, J.K.; Chen, Z.; Shen, J. Synthesis of fluorescent α -chymotrypsin A-functionalized gold nanoclusters and their application to blot-based technology for Hg²⁺ detection. *RSC Adv.* **2014**, *4*, 31536–31543. [[CrossRef](#)]

51. Senthamizhan, A.; Celebioglu, A.; Uyar, T. Real-time selective visual monitoring of Hg²⁺ detection at ppt level: An approach to lighting electrospun nanofibers using gold nanoclusters. *Sci. Rep.* **2015**, *5*, 10403. [[CrossRef](#)] [[PubMed](#)]
52. Li, X.-J.; Ling, J.; Han, C.-L.; Chen, L.-Q.; Cao, Q.-E.; Ding, Z.-T. Chicken Egg White-stabilized Au Nanoclusters for Selective and Sensitive Detection of Hg(II). *Anal. Sci.* **2017**, *33*, 671–675. [[CrossRef](#)] [[PubMed](#)]
53. Chen, S.; Kuang, Y.; Zhang, P.; Huang, Y.; Wen, A.; Zeng, X.; Feng, R.; Nie, H.; Jiang, X.; Long, Y. A dual-functional spectroscopic probe for simultaneous monitoring Cu²⁺ and Hg²⁺ ions by two different sensing nature based on novel fluorescent gold nanoclusters. *Sens. Actuators B* **2017**, *253*, 283–291. [[CrossRef](#)]
54. Yang, L.; Chen, J.; Huang, T.; Huang, L.; Sun, Z.; Jiang, Y.; Yao, T.; Wei, S. Red-emitting Au₇ nanoclusters with fluorescence sensitivity to Fe²⁺ ions. *J. Mater. Chem. C* **2017**, *5*, 4448–4454. [[CrossRef](#)]
55. Sun, J.; Zhang, J.; Jin, Y. 11-Mercaptoundecanoic acid directed one-pot synthesis of water-soluble fluorescent gold nanoclusters and their use as probes for sensitive and selective detection of Cr³⁺ and Cr⁶⁺. *J. Mater. Chem. C* **2013**, *1*, 138–143. [[CrossRef](#)]
56. Baral, A.; Basu, K.; Roy, S.; Banerjee, A. Blue Emitting Gold Cluster formation from Gold Nanorods: Selective and Sensitive Detection of Iron(III) ions in Aqueous Medium. *ACS Sustain. Chem. Eng.* **2017**, *5*, 1628–1637. [[CrossRef](#)]
57. Li, H.-W.; Yue, Y.; Liu, T.-Y.; Li, D.; Wu, Y. Fluorescence-Enhanced Sensing Mechanism of BSA-Protected Small Gold-Nanoclusters to Silver(I) Ions in Aqueous Solutions. *J. Phys. Chem. C* **2013**, *117*, 16159–16165. [[CrossRef](#)]
58. Liu, Y.; Ai, K.; Cheng, X.; Huo, L.; Lu, L. Gold-Nanocluster-Based Fluorescent Sensors for Highly Sensitive and Selective Detection of Cyanide in Water. *Adv. Funct. Mater.* **2010**, *20*, 951–956. [[CrossRef](#)]
59. Zhang, G.; Qiao, Y.; Xu, T.; Zhang, C.; Zhang, Y.; Shi, L.; Shuang, S.; Dong, C. Highly selective and sensitive nanoprobe for cyanide based on gold nanoclusters with red fluorescence emission. *Nanoscale* **2015**, *7*, 12666–12672. [[CrossRef](#)] [[PubMed](#)]
60. Shojaeifard, Z.; Hemmateenejad, B.; Shamsipur, M. Efficient On–Off Ratiometric Fluorescence Probe for Cyanide Ion Based on Perturbation of the Interaction between Gold Nanoclusters and a Copper(II)-Phthalocyanine Complex. *ACS Appl. Mater. Interfaces* **2016**, *8*, 15177–15186. [[CrossRef](#)] [[PubMed](#)]
61. Gopu, C.L.; Shanti Krishna, A.; Sreenivasan, K. Fluorimetric detection of hypochlorite using albumin stabilized gold nanoclusters. *Sens. Actuators B* **2015**, *209*, 798–802. [[CrossRef](#)]
62. Cui, M.-L.; Liu, J.-M.; Wang, X.-X.; Lin, L.-P.; Jiao, L.; Zheng, Z.-Y.; Zhang, L.-H.; Jiang, S.-L. A promising gold nanocluster fluorescent sensor for the highly sensitive and selective detection of S²⁻. *Sens. Actuators B* **2013**, *188*, 53–58. [[CrossRef](#)]
63. Liu, H.; Yang, G.; Abdel-Halim, E.S.; Zhu, J.-J. Highly selective and ultrasensitive detection of nitrite based on fluorescent gold nanoclusters. *Talanta* **2013**, *104*, 135–139. [[CrossRef](#)] [[PubMed](#)]
64. Liu, J.-M.; Cui, M.-L.; Jiang, S.-L.; Wang, X.-X.; Lin, L.-P.; Jiao, L.; Zhang, L.-H.; Zheng, Z.-Y. BSA-protected gold nanoclusters as fluorescent sensor for selective and sensitive detection of pyrophosphate. *Anal. Methods* **2013**, *5*, 3942–3947. [[CrossRef](#)]
65. Sun, J.; Yang, F.; Yang, X. Synthesis of functionalized fluorescent gold nanoclusters for acid phosphatase sensing. *Nanoscale* **2015**, *7*, 16372–16380. [[CrossRef](#)] [[PubMed](#)]
66. Zhang, Y.; Li, M.; Niu, Q.; Gao, P.; Zhang, G.; Dong, C.; Shuang, S. Gold nanoclusters as fluorescent sensors for selective and sensitive hydrogen sulfide detection. *Talanta* **2017**, *171*, 143–151. [[CrossRef](#)] [[PubMed](#)]
67. Chen, X.; Baker, G.A. Cholesterol determination using protein-templated fluorescent gold nanocluster probes. *Analyst* **2013**, *138*, 7299–7302. [[CrossRef](#)] [[PubMed](#)]
68. Govindaraju, S.; Ankireddy, S.R.; Viswanath, B.; Kim, J.; Yun, K. Fluorescent Gold Nanoclusters for Selective Detection of Dopamine in Cerebrospinal fluid. *Sci. Rep.* **2017**, *7*, 40298. [[CrossRef](#)] [[PubMed](#)]
69. Wen, F.; Dong, Y.; Feng, L.; Wang, S.; Zhang, S.; Zhang, X. Horseradish Peroxidase Functionalized Fluorescent Gold Nanoclusters for Hydrogen Peroxide Sensing. *Anal. Chem.* **2011**, *83*, 1193–1196. [[CrossRef](#)] [[PubMed](#)]
70. He, Y.; Wang, X.; Zhu, J.; Zhong, S.; Song, G. Ni²⁺-modified gold nanoclusters for fluorescence turn-on detection of histidine in biological fluids. *Analyst* **2012**, *137*, 4005–4009. [[CrossRef](#)] [[PubMed](#)]

71. Dai, H.; Shi, Y.; Wang, Y.; Sun, Y.; Hu, J.; Ni, P.; Li, Z. Label-free turn-on fluorescent detection of melamine based on the anti-quenching ability of Hg^{2+} to gold nanoclusters. *Biosens. Bioelectron.* **2014**, *53*, 76–81. [[CrossRef](#)] [[PubMed](#)]
72. Song, W.; Liang, R.-P.; Wang, Y.; Zhang, L.; Qiu, J.-D. Green synthesis of peptide-templated gold nanoclusters as novel fluorescence probes for detecting protein kinase activity. *Chem. Commun.* **2015**, *51*, 10006–10009. [[CrossRef](#)] [[PubMed](#)]
73. Chen, Z.; Qian, S.; Chen, J.; Chen, X. Highly fluorescent gold nanoclusters based sensor for the detection of quercetin. *J. Nanopart. Res.* **2012**, *14*, 1264. [[CrossRef](#)]
74. Li, S.; Huang, P.; Wu, F. Highly selective and sensitive detection of heparin based on competition-modulated assembly and disassembly of fluorescent gold nanoclusters. *New J. Chem.* **2017**, *41*, 717–723. [[CrossRef](#)]
75. Shang, L.; Nienhaus, G.U. Gold nanoclusters as novel optical probes for in vitro and in vivo fluorescence imaging. *Biophys. Rev.* **2012**, *4*, 313–322. [[CrossRef](#)] [[PubMed](#)]
76. Venkatesh, V.; Shukla, A.; Sivakumar, S.; Verma, S. Purine-Stabilized Green Fluorescent Gold Nanoclusters for Cell Nuclei Imaging Applications. *ACS Appl. Mater. Interfaces* **2014**, *6*, 2185–2191. [[CrossRef](#)] [[PubMed](#)]
77. Wang, Y.; Chen, J.-T.; Yan, X.-P. Fabrication of Transferrin Functionalized Gold Nanoclusters/Graphene Oxide Nanocomposite for Turn-On Near-Infrared Fluorescent Bioimaging of Cancer Cells and Small Animals. *Anal. Chem.* **2013**, *85*, 2529–2535. [[CrossRef](#)] [[PubMed](#)]
78. Barman, A.K.; Chaturvedi, A.; Subramaniam, K.; Verma, S. Imaging *C. elegans* with thiolated tryptophan-based NIR fluorescent gold nanoclusters. *J. Nanopart. Res.* **2013**, *15*, 2083. [[CrossRef](#)]
79. Zhou, W.; Cao, Y.; Sui, D.; Guan, W.; Lu, C.; Xie, J. Ultrastable BSA-capped gold nanoclusters with a polymer-like shielding layer against reactive oxygen species in living cells. *Nanoscale* **2016**, *8*, 9614–9620. [[CrossRef](#)] [[PubMed](#)]
80. Biswas, A.; Banerjee, S.; Gart, E.V.; Nagaraja, A.T.; McShane, M.J. Gold Nanocluster Containing Polymeric Microcapsules for Intracellular Ratiometric Fluorescence Biosensing. *ACS Omega* **2017**, *2*, 2499–2506. [[CrossRef](#)]
81. Han, Y.; Ding, C.; Zhou, J.; Tian, Y. Single Probe for Imaging and Biosensing of pH, Cu^{2+} Ions, and pH/ Cu^{2+} in Live Cells with Ratiometric Fluorescence Signals. *Anal. Chem.* **2015**, *87*, 5333–5339. [[CrossRef](#)] [[PubMed](#)]
82. Deng, H.-H.; Wu, G.-W.; Zou, Z.-Q.; Peng, H.-P.; Liu, A.-L.; Lin, X.-H.; Xia, X.-H.; Chen, W. pH-Sensitive gold nanoclusters: Preparation and analytical applications for urea, urease, and urease inhibitor detection. *Chem. Commun.* **2015**, *51*, 7847–7850. [[CrossRef](#)] [[PubMed](#)]
83. Wu, Y.-T.; Shanmugam, C.; Tseng, W.-B.; Hsieh, M.-M.; Tseng, W.-L. A gold nanocluster-based fluorescent probe for simultaneous pH and temperature sensing and its application to cellular imaging and logic gates. *Nanoscale* **2016**, *8*, 11210–11216. [[CrossRef](#)] [[PubMed](#)]
84. Ali, R.; Saleh, S.M.; Aly, S.M. Fluorescent gold nanoclusters as pH sensors for the pH 5 to 9 range and for imaging of blood cell pH values. *Microchim. Acta* **2017**, *184*, 3309–3315. [[CrossRef](#)]
85. Ghosh, S.; Anand, U.; Mukherjee, S. Luminescent Silver Nanoclusters Acting as a Label-Free Photoswitch in Metal Ion Sensing. *Anal. Chem.* **2014**, *86*, 3188–3194. [[CrossRef](#)] [[PubMed](#)]
86. Shang, L.; Dong, S. Silver nanocluster-based fluorescent sensors for sensitive detection of $\text{Cu}(\text{II})$. *J. Mater. Chem.* **2008**, *18*, 4636–4640. [[CrossRef](#)]
87. Yuan, Z.; Cai, N.; Du, Y.; He, Y.; Yeung, E.S. Sensitive and Selective Detection of Copper Ions with Highly Stable Polyethyleneimine-Protected Silver Nanoclusters. *Anal. Chem.* **2014**, *86*, 419–426. [[CrossRef](#)] [[PubMed](#)]
88. Ma, F.; Liang, S.; Peng, Y.; Kuang, Y.; Zhang, X.; Chen, S.; Long, Y.; Zeng, R. Copper ion detection using novel silver nanoclusters stabilized with amido black 10B. *Anal. Bioanal. Chem.* **2016**, *408*, 3239–3246. [[CrossRef](#)] [[PubMed](#)]
89. Sun, Z.; Li, S.; Jiang, Y.; Qiao, Y.; Zhang, L.; Xu, L.; Liu, J.; Qi, W.; Wang, H. Silver Nanoclusters with Specific Ion Recognition Modulated by Ligand Passivation toward Fluorimetric and Colorimetric Copper Analysis and Biological Imaging. *Sci. Rep.* **2016**, *6*, 20553. [[CrossRef](#)] [[PubMed](#)]
90. Adhikari, B.; Banerjee, A. Facile Synthesis of Water-Soluble Fluorescent Silver Nanoclusters and Hg^{II} Sensing. *Chem. Mater.* **2010**, *22*, 4364–4371. [[CrossRef](#)]
91. MacLean, J.L.; Morishita, K.; Liu, J. DNA stabilized silver nanoclusters for ratiometric and visual detection of Hg^{2+} and its immobilization in hydrogels. *Biosens. Bioelectron.* **2013**, *48*, 82–86. [[CrossRef](#)] [[PubMed](#)]
92. Yin, J.; He, X.; Jia, X.; Wang, K.; Xu, F. Highly sensitive label-free fluorescent detection of Hg^{2+} ions by DNA molecular machine-based Ag nanoclusters. *Analyst* **2013**, *138*, 2350–2356. [[CrossRef](#)] [[PubMed](#)]

93. Lee, J.; Park, J.; Hee Lee, H.; Park, H.; Kim, H.I.; Kim, W.J. Fluorescence switch for silver ion detection utilizing dimerization of DNA-Ag nanoclusters. *Biosens. Bioelectron.* **2015**, *68*, 642–647. [[CrossRef](#)] [[PubMed](#)]
94. Xu, N.; Zhu, Q.; Kong, X.-Y.; Meng, L. A sensitive detection of Cr(vi) in wide pH range using polyethyleneimine protected silver nanoclusters. *Anal. Methods* **2016**, *8*, 5684–5689. [[CrossRef](#)]
95. Chen, Z.; Lu, D.; Zhang, G.; Yang, J.; Dong, C.; Shuang, S. Glutathione capped silver nanoclusters-based fluorescent probe for highly sensitive detection of Fe³⁺. *Sens. Actuators B* **2014**, *202*, 631–637. [[CrossRef](#)]
96. Wang, C.; Wu, J.; Jiang, K.; Humphrey, M.G.; Zhang, C. Stable Ag nanoclusters-based nano-sensors: Rapid sonochemical synthesis and detecting Pb²⁺ in living cells. *Sens. Actuators B* **2017**, *238*, 1136–1143. [[CrossRef](#)]
97. Liu, X.; Wang, L.; Zhang, N.; Shangguan, D. Ratiometric fluorescent silver nanoclusters for the determination of mercury and copper ions. *Anal. Methods* **2015**, *7*, 8019–8024. [[CrossRef](#)]
98. Zhou, T.; Rong, M.; Cai, Z.; Yang, C.J.; Chen, X. Sonochemical synthesis of highly fluorescent glutathione-stabilized Ag nanoclusters and S²⁻ sensing. *Nanoscale* **2012**, *4*, 4103–4106. [[CrossRef](#)] [[PubMed](#)]
99. Gao, Z.; Liu, F.; Hu, R.; Zhao, M.; Shao, N. Lysozyme-stabilized Ag nanoclusters: Synthesis of different compositions and fluorescent responses to sulfide ions with distinct modes. *RSC Adv.* **2016**, *6*, 66233–66241. [[CrossRef](#)]
100. Huang, X.; Shahzad, S.A.; Li, Y.; Zhang, Y.; Sang, L.; Zhou, H.; Jiang, H.; Kam-Wing Lo, K.; Yu, C. Silver nanoclusters capped silica nanoparticles as a ratiometric photoluminescence nanosensor for the selective detection of I⁻ and S²⁻. *Anal. Chim. Acta* **2017**, *988*, 74–80. [[CrossRef](#)] [[PubMed](#)]
101. Chen, C.; Yuan, Z.; Chang, H.-T.; Lu, F.; Li, Z.; Lu, C. Silver nanoclusters as fluorescent nanosensors for selective and sensitive nitrite detection. *Anal. Methods* **2016**, *8*, 2628–2633. [[CrossRef](#)]
102. Feng, L.; Sun, Z.; Liu, H.; Liu, M.; Jiang, Y.; Fan, C.; Cai, Y.; Zhang, S.; Xu, J.; Wang, H. Silver nanoclusters with enhanced fluorescence and specific ion recognition capability triggered by alcohol solvents: A highly selective fluorimetric strategy for detecting iodide ions in urine. *Chem. Commun.* **2017**, *53*, 9466–9469. [[CrossRef](#)] [[PubMed](#)]
103. Fu, L.; Li, C.; Li, Y.; Chen, S.; Long, Y.; Zeng, R. Simultaneous determination of iodide and bromide using a novel LSPR fluorescent Ag nanocluster probe. *Sens. Actuators B* **2017**, *240*, 315–321. [[CrossRef](#)]
104. Liu, F.; Bing, T.; Shangguan, D.; Zhao, M.; Shao, N. Ratiometric Fluorescent Biosensing of Hydrogen Peroxide and Hydroxyl Radical in Living Cells with Lysozyme–Silver Nanoclusters: Lysozyme as Stabilizing Ligand and Fluorescence Signal Unit. *Anal. Chem.* **2016**, *88*, 10631–10638. [[CrossRef](#)] [[PubMed](#)]
105. Liu, T.; Su, Y.; Song, H.; Lv, Y. Microwave-assisted green synthesis of ultrasmall fluorescent water-soluble silver nanoclusters and its application in chiral recognition of amino acids. *Analyst* **2013**, *138*, 6558–6564. [[CrossRef](#)] [[PubMed](#)]
106. Huang, Z.; Pu, F.; Lin, Y.; Ren, J.; Qu, X. Modulating DNA-templated silver nanoclusters for fluorescence turn-on detection of thiol compounds. *Chem. Commun.* **2011**, *47*, 3487–3489. [[CrossRef](#)] [[PubMed](#)]
107. Zhang, N.; Qu, F.; Luo, H.Q.; Li, N.B. Sensitive and selective detection of biothiols based on target-induced agglomeration of silver nanoclusters. *Biosens. Bioelectron.* **2013**, *42*, 214–218. [[CrossRef](#)] [[PubMed](#)]
108. Yuan, X.; Tay, Y.; Dou, X.; Luo, Z.; Leong, D.T.; Xie, J. Glutathione-Protected Silver Nanoclusters as Cysteine-Selective Fluorometric and Colorimetric Probe. *Anal. Chem.* **2013**, *85*, 1913–1919. [[CrossRef](#)] [[PubMed](#)]
109. Zhu, J.; Song, X.; Gao, L.; Li, Z.; Liu, Z.; Ding, S.; Zou, S.; He, Y. A highly selective sensor of cysteine with tunable sensitivity and detection window based on dual-emission Ag nanoclusters. *Biosens. Bioelectron.* **2014**, *53*, 71–75. [[CrossRef](#)] [[PubMed](#)]
110. Dong, J.X.; Gao, Z.F.; Zhang, Y.; Li, B.L.; Zhang, W.; Lei, J.L.; Li, N.B.; Luo, H.Q. The pH-switchable agglomeration and dispersion behavior of fluorescent Ag nanoclusters and its applications in urea and glucose biosensing. *NPG Asia Mater.* **2016**, *8*, e335. [[CrossRef](#)]
111. Ren, H.; Li, M.; Fu, Y.; Jin, L. Silver nanoclusters functionalized by chromotropic acid and layered double hydroxides for the turn-on detection of melamine. *J. Mater. Chem. C* **2016**, *4*, 6104–6109. [[CrossRef](#)]
112. Chen, Y.; Sun, Y.; Song, R.; Song, S.; Zhao, Y.; Yang, X.; Yu, C.; Lin, Q. Fluorometric “Turn-On” glucose sensing through the in situ generation of silver nanoclusters. *RSC Adv.* **2017**, *7*, 1396–1400. [[CrossRef](#)]
113. Mao, B.; Qu, F.; Zhu, S.; You, J. Fluorescence turn-on strategy based on silver nanoclusters–Cu²⁺ system for trace detection of quinolones. *Sens. Actuators B* **2016**, *234*, 338–344. [[CrossRef](#)]

114. Sharma, J.; Yeh, H.-C.; Yoo, H.; Werner, J.H.; Martinez, J.S. Silver nanocluster aptamers: In situ generation of intrinsically fluorescent recognition ligands for protein detection. *Chem. Commun.* **2011**, *47*, 2294–2296. [[CrossRef](#)] [[PubMed](#)]
115. Zhou, Y.W.; Li, C.M.; Liu, Y.; Huang, C.Z. Effective detection and cell imaging of prion protein with new prepared targetable yellow-emission silver nanoclusters. *Analyst* **2013**, *138*, 873–878. [[CrossRef](#)] [[PubMed](#)]
116. Chang, Y.; Zhang, P.; Yu, Y.; Du, Y.Q.; Wang, W.; Huang, C.Z. DNA-templated silver nanoclusters as label-free fluorescent probes for detection of bleomycin. *Anal. Methods* **2013**, *5*, 6200–6204. [[CrossRef](#)]
117. Basiruddin, S.K.; Chakraborty, A. One step synthesis of maltose functionalized red fluorescent Ag cluster for specific glycoprotein detection and cellular imaging probe. *RSC Adv.* **2014**, *4*, 43098–43104. [[CrossRef](#)]
118. Yang, S.W.; Vosch, T. Rapid Detection of MicroRNA by a Silver Nanocluster DNA Probe. *Anal. Chem.* **2011**, *83*, 6935–6939. [[CrossRef](#)] [[PubMed](#)]
119. Liu, Y.-Q.; Zhang, M.; Yin, B.-C.; Ye, B.-C. Attomolar Ultrasensitive MicroRNA Detection by DNA-Scaffolded Silver-Nanocluster Probe Based on Isothermal Amplification. *Anal. Chem.* **2012**, *84*, 5165–5169. [[CrossRef](#)] [[PubMed](#)]
120. Wang, G.; Zhu, Y.; Chen, L.; Wang, L.; Zhang, X. Target-induced quenching for highly sensitive detection of nucleic acids based on label-free luminescent supersandwich DNA/silver nanoclusters. *Analyst* **2014**, *139*, 165–169. [[CrossRef](#)] [[PubMed](#)]
121. Zhang, Y.; Zhu, C.; Zhang, L.; Tan, C.; Yang, J.; Chen, B.; Wang, L.; Zhang, H. DNA-Templated Silver Nanoclusters for Multiplexed Fluorescent DNA Detection. *Small* **2015**, *11*, 1385–1389. [[CrossRef](#)] [[PubMed](#)]
122. Zhu, J.; Zhang, L.; Teng, Y.; Lou, B.; Jia, X.; Gu, X.; Wang, E. G-quadruplex enhanced fluorescence of DNA-silver nanoclusters and their application in bioimaging. *Nanoscale* **2015**, *7*, 13224–13229. [[CrossRef](#)] [[PubMed](#)]
123. Le Guével, X.; Spies, C.; Daum, N.; Jung, G.; Schneider, M. Highly fluorescent silver nanoclusters stabilized by glutathione: A promising fluorescent label for bioimaging. *Nano Res.* **2012**, *5*, 379–387. [[CrossRef](#)]
124. Qu, F.; Li, N.B.; Luo, H.Q. Highly Sensitive Fluorescent and Colorimetric pH Sensor Based on Polyethylenimine-Capped Silver Nanoclusters. *Langmuir* **2013**, *29*, 1199–1205. [[CrossRef](#)] [[PubMed](#)]
125. Mao, M.; Deng, C.; He, Y.; Ge, Y.; Song, G. Fluorescence Detection of p-Nitrophenol in Water Using Bovine Serum Albumin Capped ag Nanoclusters. *J. Fluoresc.* **2017**, *27*, 1421–1426. [[CrossRef](#)] [[PubMed](#)]
126. Enkin, N.; Sharon, E.; Golub, E.; Willner, I. Ag Nanocluster/DNA Hybrids: Functional Modules for the Detection of Nitroaromatic and RDX Explosives. *Nano Lett.* **2014**, *14*, 4918–4922. [[CrossRef](#)] [[PubMed](#)]
127. Cao, H.; Chen, Z.; Zheng, H.; Huang, Y. Copper nanoclusters as a highly sensitive and selective fluorescence sensor for ferric ions in serum and living cells by imaging. *Biosens. Bioelectron.* **2014**, *62*, 189–195. [[CrossRef](#)] [[PubMed](#)]
128. Das, N.K.; Ghosh, S.; Priya, A.; Datta, S.; Mukherjee, S. Luminescent Copper Nanoclusters as a Specific Cell-Imaging Probe and a Selective Metal Ion Sensor. *J. Phys. Chem. C* **2015**, *119*, 24657–24664. [[CrossRef](#)]
129. Liu, Z.-C.; Qi, J.-W.; Hu, C.; Zhang, L.; Song, W.; Liang, R.-P.; Qiu, J.-D. Cu nanoclusters-based ratiometric fluorescence probe for ratiometric and visualization detection of copper ions. *Anal. Chimica Acta* **2015**, *895*, 95–103. [[CrossRef](#)] [[PubMed](#)]
130. Hu, X.; Wang, W.; Huang, Y. Copper nanocluster-based fluorescent probe for sensitive and selective detection of Hg²⁺ in water and food stuff. *Talanta* **2016**, *154*, 409–415. [[CrossRef](#)] [[PubMed](#)]
131. Wang, C.; Cheng, H.; Huang, Y.; Xu, Z.; Lin, H.; Zhang, C. Facile sonochemical synthesis of pH-responsive copper nanoclusters for selective and sensitive detection of Pb²⁺ in living cells. *Analyst* **2015**, *140*, 5634–5639. [[CrossRef](#)] [[PubMed](#)]
132. Han, B.-Y.; Hou, X.-F.; Xiang, R.-C.; Yu, M.-B.; Li, Y.; Peng, T.-T.; He, G.-H. Detection of Lead Ion Based on Aggregation-induced Emission of Copper Nanoclusters. *Chin. J. Anal. Chem.* **2017**, *45*, 23–27. [[CrossRef](#)]
133. Goswami, N.; Giri, A.; Bootharaju, M.S.; Xavier, P.L.; Pradeep, T.; Pal, S.K. Copper Quantum Clusters in Protein Matrix: Potential Sensor of Pb²⁺ Ion. *Anal. Chem.* **2011**, *83*, 9676–9680. [[CrossRef](#)] [[PubMed](#)]
134. Hu, X.; Mao, X.; Zhang, X.; Huang, Y. One-step synthesis of orange fluorescent copper nanoclusters for sensitive and selective sensing of Al³⁺ ions in food samples. *Sens. Actuators B* **2017**, *247*, 312–318. [[CrossRef](#)]
135. Lin, L.; Hu, Y.; Zhang, L.; Huang, Y.; Zhao, S. Photoluminescence light-up detection of zinc ion and imaging in living cells based on the aggregation induced emission enhancement of glutathione-capped copper nanoclusters. *Biosens. Bioelectron.* **2017**, *94*, 523–529. [[CrossRef](#)] [[PubMed](#)]

136. Li, Z.; Guo, S.; Lu, C. A highly selective fluorescent probe for sulfide ions based on aggregation of Cu nanocluster induced emission enhancement. *Analyst* **2015**, *140*, 2719–2725. [[CrossRef](#)] [[PubMed](#)]
137. Khonkayan, K.; Sansuk, S.; Srijaranai, S.; Tuntulani, T.; Saiyasombat, C.; Busayaporn, W.; Ngeontae, W. New approach for detection of chromate ion by preconcentration with mixed metal hydroxide coupled with fluorescence sensing of copper nanoclusters. *Microchim. Acta* **2017**, *184*, 2965–2974. [[CrossRef](#)]
138. Zhong, Y.; Wang, Q.; He, Y.; Ge, Y.; Song, G. A novel fluorescence and naked eye sensor for iodide in urine based on the iodide induced oxidative etching and aggregation of Cu nanoclusters. *Sens. Actuators B* **2015**, *209*, 147–153. [[CrossRef](#)]
139. Zheng, X.-J.; Liang, R.-P.; Li, Z.-J.; Zhang, L.; Qiu, J.-D. One-step, stabilizer-free and green synthesis of Cu nanoclusters as fluorescent probes for sensitive and selective detection of nitrite ions. *Sens. Actuators B* **2016**, *230*, 314–319. [[CrossRef](#)]
140. Zhou, D.-L.; Huang, H.; Wang, Y. Sensitive and selective detection of nitrite ions with highly fluorescent glutathione-stabilized copper nanoclusters. *Anal. Methods* **2017**, *9*, 5668–5673. [[CrossRef](#)]
141. Cang, J.; Wang, C.-W.; Chen, P.-C.; Lin, Y.-J.; Li, Y.-C.; Chang, H.-T. Control of pH for separated quantitation of nitrite and cyanide ions using photoluminescent copper nanoclusters. *Anal. Methods* **2017**, *9*, 5254–5259. [[CrossRef](#)]
142. Wang, W.; Zhan, L.; Du, Y.Q.; Leng, F.; Huang, C.Z. A new spectrofluorometric method for pyrophosphate assay based on the fluorescence enhancement of trypsin-stabilized copper clusters. *Anal. Methods* **2015**, *7*, 638–642. [[CrossRef](#)]
143. Hu, Y.; Wu, Y.; Chen, T.; Chu, X.; Yu, R. Double-strand DNA-templated synthesis of copper nanoclusters as novel fluorescence probe for label-free detection of biothiols. *Anal. Methods* **2013**, *5*, 3577–3581. [[CrossRef](#)]
144. Hu, L.; Yuan, Y.; Zhang, L.; Zhao, J.; Majeed, S.; Xu, G. Copper nanoclusters as peroxidase mimetics and their applications to H₂O₂ and glucose detection. *Anal. Chim. Acta* **2013**, *762*, 83–86. [[CrossRef](#)] [[PubMed](#)]
145. Zhao, X.J.; Huang, C.Z. Water-soluble luminescent copper nanoclusters reduced and protected by histidine for sensing of guanosine 5'-triphosphate. *New J. Chem.* **2014**, *38*, 3673–3677. [[CrossRef](#)]
146. Wang, Y.-M.; Liu, J.-W.; Duan, L.-Y.; Liu, S.-J.; Jiang, J.-H. Aptamer-based fluorometric determination of ATP by using target-cycling strand displacement amplification and copper nanoclusters. *Microchim. Acta* **2017**, *184*, 4183–4188. [[CrossRef](#)]
147. Wang, C.; Shu, S.; Yao, Y.; Song, Q. A fluorescent biosensor of lysozyme-stabilized copper nanoclusters for the selective detection of glucose. *RSC Adv.* **2015**, *5*, 101599–101606. [[CrossRef](#)]
148. Borghei, Y.-S.; Hosseini, M.; Khoobi, M.; Ganjali, M.R. Novel Fluorometric Assay for Detection of Cysteine as a Reducing Agent and Template in Formation of Copper Nanoclusters. *J. Fluoresc.* **2017**, *27*, 529–536. [[CrossRef](#)] [[PubMed](#)]
149. Li, X.-G.; Zhang, F.; Gao, Y.; Zhou, Q.-M.; Zhao, Y.; Li, Y.; Huo, J.-Z.; Zhao, X.-J. Facile synthesis of red emitting 3-aminophenylboronic acid functionalized copper nanoclusters for rapid, selective and highly sensitive detection of glycoproteins. *Biosens. Bioelectron.* **2016**, *86*, 270–276. [[CrossRef](#)] [[PubMed](#)]
150. Zhao, M.; Qian, Z.; Zhong, M.; Chen, Z.; Ao, H.; Feng, H. Fabrication of Stable and Luminescent Copper Nanocluster-Based AIE Particles and Their Application in β -Galactosidase Activity Assay. *ACS Appl. Mater. Interfaces* **2017**, *9*, 32887–32895. [[CrossRef](#)] [[PubMed](#)]
151. Wang, X.-P.; Yin, B.-C.; Ye, B.-C. A novel fluorescence probe of dsDNA-templated copper nanoclusters for quantitative detection of microRNAs. *RSC Adv.* **2013**, *3*, 8633–8636. [[CrossRef](#)]
152. Borghei, Y.-S.; Hosseini, M.; Ganjali, M.R. Fluorescence based turn-on strategy for determination of microRNA-155 using DNA-templated copper nanoclusters. *Microchim. Acta* **2017**, *184*, 2671–2677. [[CrossRef](#)]
153. Huang, H.; Li, H.; Wang, A.-J.; Zhong, S.-X.; Fang, K.-M.; Feng, J.-J. Green synthesis of peptide-templated fluorescent copper nanoclusters for temperature sensing and cellular imaging. *Analyst* **2014**, *139*, 6536–6541. [[CrossRef](#)] [[PubMed](#)]
154. Basu, K.; Gayen, K.; Mitra, T.; Baral, A.; Roy, S.S.; Banerjee, A. Different Color Emissive Copper Nanoclusters for Cancer Cell Imaging. *ChemNanoMat* **2017**, *3*, 808–814. [[CrossRef](#)]
155. Wang, W.; Leng, F.; Zhan, L.; Chang, Y.; Yang, X.X.; Lan, J.; Huang, C.Z. One-step prepared fluorescent copper nanoclusters for reversible pH-sensing. *Analyst* **2014**, *139*, 2990–2993. [[CrossRef](#)] [[PubMed](#)]
156. Zhang, G.; Xu, T.; Du, H.; Qiao, Y.; Guo, X.; Shi, L.; Zhang, Y.; Shuang, S.; Dong, C.; Ma, H. A reversible fluorescent pH-sensing system based on the one-pot synthesis of natural silk fibroin-capped copper nanoclusters. *J. Mater. Chem. C* **2016**, *4*, 3540–3545. [[CrossRef](#)]

157. Deng, X.; Huang, X.; Wu, D. Förster resonance-energy-transfer detection of 2,4,6-trinitrophenol using copper nanoclusters. *Anal. Bioanal. Chem.* **2015**, *407*, 4607–4613. [[CrossRef](#)] [[PubMed](#)]
158. Wang, Z.; Chen, R.; Xiong, Y.; Cepe, K.; Schneider, J.; Zboril, R.; Lee, C.-S.; Rogach, A.L. Incorporating Copper Nanoclusters into Metal-Organic Frameworks: Confinement-Assisted Emission Enhancement and Application for Trinitrotoluene Detection. *Part. Part. Syst. Charact.* **2017**, *34*. [[CrossRef](#)]
159. Huang, Y.; Liu, W.; Feng, H.; Ye, Y.; Tang, C.; Ao, H.; Zhao, M.; Chen, G.; Chen, J.; Qian, Z. Luminescent Nanoswitch Based on Organic-Phase Copper Nanoclusters for Sensitive Detection of Trace Amount of Water in Organic Solvents. *Anal. Chem.* **2016**, *88*, 7429–7434. [[CrossRef](#)] [[PubMed](#)]
160. Su, X.; Liu, J. pH-Guided Self-Assembly of Copper Nanoclusters with Aggregation-Induced Emission. *ACS Appl. Mater. Interfaces* **2017**, *9*, 3902–3910. [[CrossRef](#)] [[PubMed](#)]
161. Duchesne, P.N.; Zhang, P. Local structure of fluorescent platinum nanoclusters. *Nanoscale* **2012**, *4*, 4199–4205. [[CrossRef](#)] [[PubMed](#)]
162. George, A.; Gopalakrishnan, H.; Mandal, S. Surfactant free platinum nanocluster as fluorescent probe for the selective detection of Fe (III) ions in aqueous medium. *Sens. Actuators B* **2017**, *243*, 332–337. [[CrossRef](#)]
163. Xia, X.; Zhang, Y.; Wang, J. Novel fabrication of highly fluorescent Pt nanoclusters and their applications in hypochlorite assay. *RSC Adv.* **2014**, *4*, 25365–25368. [[CrossRef](#)]
164. Jin, L.; Meng, Z.; Zhang, Y.; Cai, S.; Zhang, Z.; Li, C.; Shang, L.; Shen, Y. Ultrasmall Pt Nanoclusters as Robust Peroxidase Mimics for Colorimetric Detection of Glucose in Human Serum. *ACS Appl. Mater. Interfaces* **2017**, *9*, 10027–10033. [[CrossRef](#)] [[PubMed](#)]
165. Xu, N.; Li, H.-W.; Wu, Y. Hydrothermal synthesis of polyethylenimine-protected high luminescent Pt-nanoclusters and their application to the detection of nitroimidazoles. *Anal. Chim. Acta* **2017**, *958*, 51–58. [[CrossRef](#)] [[PubMed](#)]
166. Chen, D.; Gao, S.; Ge, W.; Li, Q.; Jiang, H.; Wang, X. One-step rapid synthesis of fluorescent platinum nanoclusters for cellular imaging and photothermal treatment. *RSC Adv.* **2014**, *4*, 40141–40145. [[CrossRef](#)]
167. Chen, D.; Zhao, C.; Ye, J.; Li, Q.; Liu, X.; Su, M.; Jiang, H.; Amatore, C.; Selke, M.; Wang, X. In Situ Biosynthesis of Fluorescent Platinum Nanoclusters: Toward Self-Bioimaging-Guided Cancer Theranostics. *ACS Appl. Mater. Interfaces* **2015**, *7*, 18163–18169. [[CrossRef](#)] [[PubMed](#)]
168. King, N.S.; Liu, L.; Yang, X.; Cerjan, B.; Everitt, H.O.; Nordlander, P.; Halas, N.J. Fano Resonant Aluminum Nanoclusters for Plasmonic Colorimetric Sensing. *ACS Nano* **2015**, *9*, 10628–10636. [[CrossRef](#)] [[PubMed](#)]
169. Atta, N.F.; El-Kady, M.F.; Galal, A. Palladium nanoclusters-coated polyfuran as a novel sensor for catecholamine neurotransmitters and paracetamol. *Sens. Actuators B* **2009**, *141*, 566–574. [[CrossRef](#)]
170. Sarparast, M.; Noori, A.; Ilkhani, H.; Bathaie, S.Z.; El-Kady, M.F.; Wang, L.J.; Pham, H.; Marsh, K.L.; Kaner, R.B.; Mousavi, M.F. Cadmium nanoclusters in a protein matrix: Synthesis, characterization, and application in targeted drug delivery and cellular imaging. *Nano Res.* **2016**, *9*, 3229–3246. [[CrossRef](#)]
171. Vankayala, R.; Gollavelli, G.; Mandal, B.K. Highly fluorescent and biocompatible iridium nanoclusters for cellular imaging. *J. Mater. Sci.* **2013**, *24*, 1993–2000. [[CrossRef](#)] [[PubMed](#)]
172. Su, Y.-T.; Lan, G.-Y.; Chen, W.-Y.; Chang, H.-T. Detection of Copper Ions Through Recovery of the Fluorescence of DNA-Templated Copper/Silver Nanoclusters in the Presence of Mercaptopropionic Acid. *Anal. Chem.* **2010**, *82*, 8566–8572. [[CrossRef](#)] [[PubMed](#)]
173. Zhou, T.-Y.; Lin, L.-P.; Rong, M.-C.; Jiang, Y.-Q.; Chen, X. Silver–Gold Alloy Nanoclusters as a Fluorescence-Enhanced Probe for Aluminum Ion Sensing. *Anal. Chem.* **2013**, *85*, 9839–9844. [[CrossRef](#)] [[PubMed](#)]
174. Zhang, N.; Si, Y.; Sun, Z.; Chen, L.; Li, R.; Qiao, Y.; Wang, H. Rapid, Selective, and Ultrasensitive Fluorimetric Analysis of Mercury and Copper Levels in Blood Using Bimetallic Gold-Silver Nanoclusters with “Silver Effect”—Enhanced Red Fluorescence. *Anal. Chem.* **2014**, *86*, 11714–11721. [[CrossRef](#)] [[PubMed](#)]
175. Zheng, B.; Zheng, J.; Yu, T.; Sang, A.; Du, J.; Guo, Y.; Xiao, D.; Choi, M.M.F. Fast microwave-assisted synthesis of AuAg bimetallic nanoclusters with strong yellow emission and their response to mercury(II) ions. *Sens. Actuators B* **2015**, *221*, 386–392. [[CrossRef](#)]

176. Huang, H.; Li, H.; Feng, J.-J.; Wang, A.-J. One-step green synthesis of fluorescent bimetallic Au/Ag nanoclusters for temperature sensing and in vitro detection of Fe³⁺. *Sens. Actuators, B* **2016**, *223*, 550–556. [[CrossRef](#)]
177. Yang, Y.; Sun, Y.; Liao, S.; Wu, Z.; Yu, R. Bimetallic gold-silver nanocluster fluorescent probes for Cr(III) and Cr(VI). *Anal. Methods* **2016**, *8*, 7237–7241. [[CrossRef](#)]
178. Zhang, T.; Xu, H.; Xu, S.; Dong, B.; Wu, Z.; Zhang, X.; Zhang, L.; Song, H. DNA stabilized Ag-Au alloy nanoclusters and their application as sensing probes for mercury ions. *RSC Adv.* **2016**, *6*, 51609–51618. [[CrossRef](#)]
179. Ding, S.-N.; Guo, Y.-X. One-pot synthesis of dual-emitting BSA-Pt-Au bimetallic nanoclusters for fluorescence ratiometric detection of mercury ions and cysteine. *Anal. Methods* **2015**, *7*, 5787–5793. [[CrossRef](#)]
180. Wang, Z.-X.; Guo, Y.-X.; Ding, S.-N. Fluorometric determination of cadmium(II) and mercury(II) using nanoclusters consisting of a gold-nickel alloy. *Microchim. Acta* **2015**, *182*, 2223–2231. [[CrossRef](#)]
181. Chen, W.-Y.; Lan, G.-Y.; Chang, H.-T. Use of Fluorescent DNA-Templated Gold/Silver Nanoclusters for the Detection of Sulfide Ions. *Anal. Chem.* **2011**, *83*, 9450–9455. [[CrossRef](#)] [[PubMed](#)]
182. Zhang, P.; Wang, Y.; Chen, L.; Yin, Y. Bimetallic nanoclusters with strong red fluorescence for sensitive detection of hypochlorite in tap water. *Microchim. Acta* **2017**, *184*, 3781–3787. [[CrossRef](#)]
183. Zhou, Q.; Lin, Y.; Xu, M.; Gao, Z.; Yang, H.; Tang, D. Facile Synthesis of Enhanced Fluorescent Gold-Silver Bimetallic Nanocluster and Its Application for Highly Sensitive Detection of Inorganic Pyrophosphatase Activity. *Anal. Chem.* **2016**, *88*, 8886–8892. [[CrossRef](#)] [[PubMed](#)]
184. Li, Z.; Liu, R.; Xing, G.; Wang, T.; Liu, S. A novel fluorometric and colorimetric sensor for iodide determination using DNA-templated gold/silver nanoclusters. *Biosens. Bioelectron.* **2017**, *96*, 44–48. [[CrossRef](#)] [[PubMed](#)]
185. Ding, Y.; Li, X.; Chen, C.; Ling, J.; Li, W.; Guo, Y.; Yan, J.; Zha, L.; Cai, J. A rapid evaluation of acute hydrogen sulfide poisoning in blood based on DNA-Cu/Ag nanocluster fluorescence probe. *Sci. Rep.* **2017**, *7*, 9638. [[CrossRef](#)] [[PubMed](#)]
186. Wang, Z.-X.; Ding, S.-N.; Jomma Narjh, E.Y. Determination of Thiols by Fluorescence using Au@Ag Nanoclusters as Probes. *Anal. Lett.* **2015**, *48*, 647–658. [[CrossRef](#)]
187. Sun, J.; Yang, F.; Zhao, D.; Chen, C.; Yang, X. Integrated Logic Gate for Fluorescence Turn-on Detection of Histidine and Cysteine Based on Ag/Au Bimetallic Nanoclusters–Cu²⁺ Ensemble. *ACS Appl. Mater. Interfaces* **2015**, *7*, 6860–6866. [[CrossRef](#)] [[PubMed](#)]
188. Feng, J.; Huang, P.; Wu, F.-Y. Gold-platinum bimetallic nanoclusters with enhanced peroxidase-like activity and their integrated agarose hydrogel-based sensing platform for the colorimetric analysis of glucose levels in serum. *Analyst* **2017**, *142*, 4106–4115. [[CrossRef](#)] [[PubMed](#)]
189. Ahn, J.K.; Kim, H.Y.; Baek, S.; Park, H.G. A new s-adenosylhomocysteine hydrolase-linked method for adenosine detection based on DNA-templated fluorescent Cu/Ag nanoclusters. *Biosens. Bioelectron.* **2017**, *93*, 330–334. [[CrossRef](#)] [[PubMed](#)]
190. Li, W.; Li, W.; Hu, Y.; Xia, Y.; Shen, Q.; Nie, Z.; Huang, Y.; Yao, S. A fluorometric assay for acetylcholinesterase activity and inhibitor detection based on DNA-templated copper/silver nanoclusters. *Biosens. Bioelectron.* **2013**, *47*, 345–349. [[CrossRef](#)] [[PubMed](#)]
191. Hu, D.-H.; Sheng, Z.-H.; Zhang, P.-F.; Yang, D.-Z.; Liu, S.-H.; Gong, P.; Gao, D.-Y.; Fang, S.-T.; Ma, Y.-F.; Cai, L.-T. Hybrid gold-gadolinium nanoclusters for tumor-targeted NIRF/CT/MRI triple-modal imaging in vivo. *Nanoscale* **2013**, *5*, 1624–1628. [[CrossRef](#)] [[PubMed](#)]
192. Dutta, D.; Chattopadhyay, A.; Ghosh, S.S. Cationic BSA Templated Au–Ag Bimetallic Nanoclusters As a Theranostic Gene Delivery Vector for HeLa Cancer Cells. *ACS Biomater. Sci. Eng.* **2016**, *2*, 2090–2098. [[CrossRef](#)]
193. Chen, L.; Zhang, Y.; Jiang, H.; Wang, X.; Liu, C. Cytidine Mediated AuAg Nanoclusters as Bright Fluorescent Probe for Tumor Imaging in vivo. *Chin. J. Chem.* **2016**, *34*, 589–593. [[CrossRef](#)]
194. Chen, P.-C.; Ma, J.-Y.; Chen, L.-Y.; Lin, G.-L.; Shih, C.-C.; Lin, T.-Y.; Chang, H.-T. Photoluminescent AuCu bimetallic nanoclusters as pH sensors and catalysts. *Nanoscale* **2014**, *6*, 3503–3507. [[CrossRef](#)] [[PubMed](#)]

195. Han, B.; Hou, X.; Xiang, R.; He, G. Synthesis of highly luminescent Cu/Ag bimetal nanoclusters and their application in a temperature sensor. *Anal. Methods* **2017**, *9*, 4028–4032. [[CrossRef](#)]
196. Goswami, N.; Yao, Q.; Luo, Z.; Li, J.; Chen, T.; Xie, J. Luminescent Metal Nanoclusters with Aggregation-Induced Emission. *J. Phys. Chem. Lett.* **2016**, *7*, 962–975. [[CrossRef](#)] [[PubMed](#)]
197. Kang, X.; Xiong, L.; Wang, S.; Yu, H.; Jin, S.; Song, Y.; Chen, T.; Zheng, L.; Pan, C.; Pei, Y.; et al. Shape-Controlled Synthesis of Trimetallic Nanoclusters: Structure Elucidation and Properties Investigation. *Chem. Eur. J.* **2016**, *22*, 17145–17150. [[CrossRef](#)] [[PubMed](#)]



© 2017 by the authors. Licensee MDPI, Basel, Switzerland. This article is an open access article distributed under the terms and conditions of the Creative Commons Attribution (CC BY) license (<http://creativecommons.org/licenses/by/4.0/>).